INTERACTION OF PROJECTILES AND COMPOSITE ARMOR. PART II

Alexander L. Florence

Stanford Research Institute
Menlo Park, California

August 1969

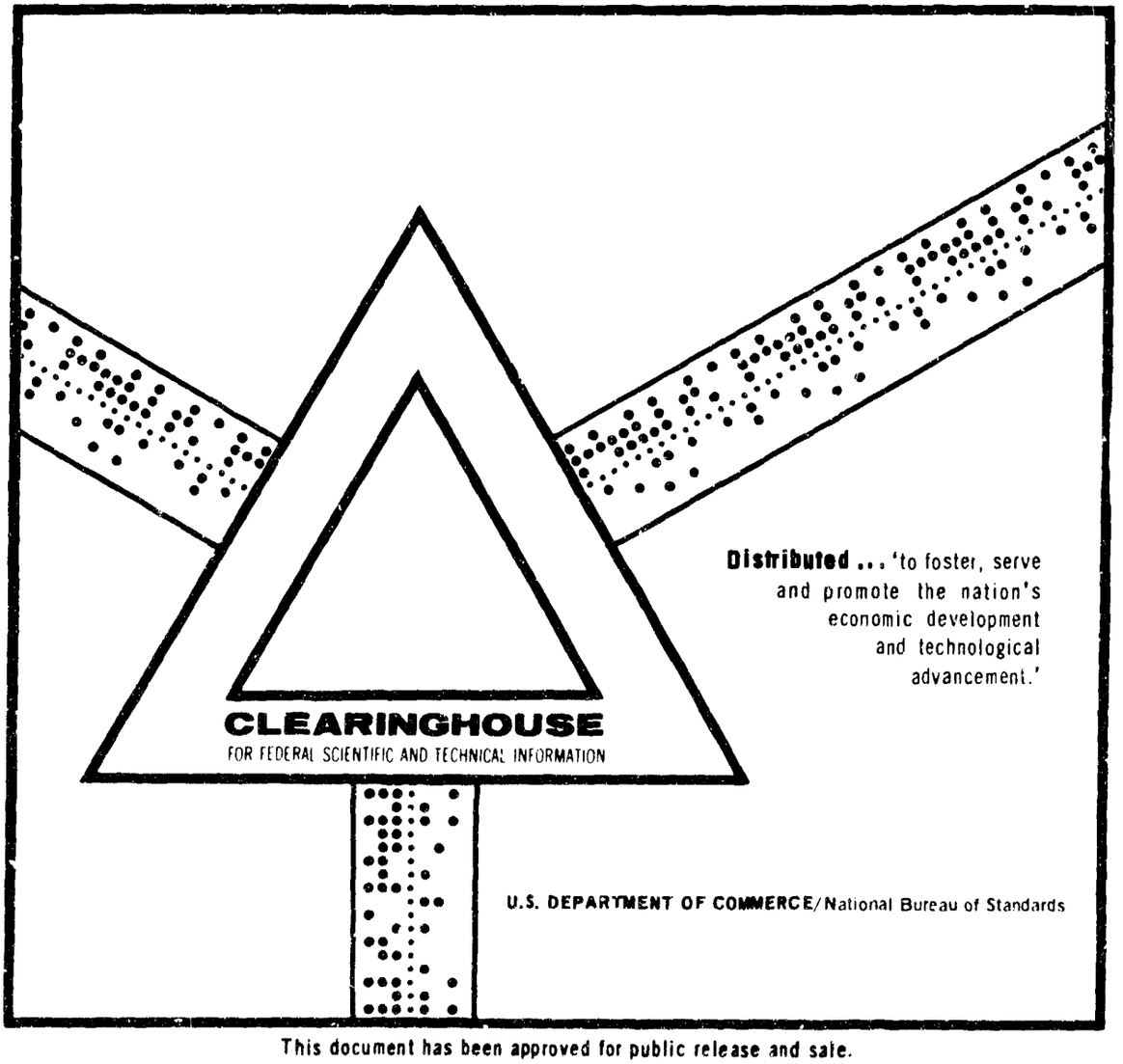

AMMRC CR 69-15

INTERACTION OF PROJECTILES AND COMPOSITE ARMOR

PART II

Final Report

by

A. L. FLORENCE

August 1969

STANFORD RESEARCH INSTITUTE
Menlo Park, California 94025

CONTRACT DAAG46-68-C-0054

ARMY MATERIALS AND MECHANICS RESEARCH CENTER
WATERTOWN, MASSACHUSETTS 02172

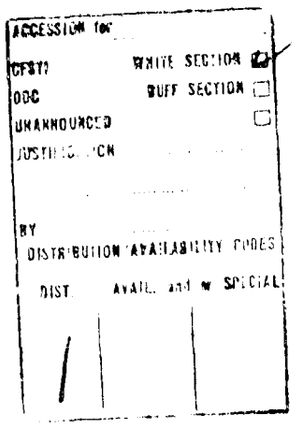

The findings in this report are not to be construed as an official Department of the Army position, unless so designated by other authorized documents.

Mention of any trade names or manufacturers in this report shall not be construed as advertising nor as an official indorsement or approval of such products or companies by the United States Government.

DISPOSITION INSTRUCTIONS

Destroy this report when it is no longer needed.
Do not return it to the originator.

INTERACTION OF PROJECTILES AND COMPOSITE ARMOR

PART II

AMMRC CR 69-15

by

A. L. FLORENCE

August 1969

Stanford Research Institute
Menlo Park, California 94025

CONTRACT DAAG46-68-C-0054
AMCMS Code No. 5122.11.1955

SRI Project PGU-7303

ARMY MATERIALS AND MECHANICS RESEARCH CENTER
WATERTOWN, MASSACHUSETTS 02172

ABSTRACT

This report describes basic experimental and theoretical investigations of the interaction of projectiles and lightweight armor. The armor of interest is a very hard and relatively inflexible facing plate (ceramic) bonded to a flexible backing plate (fiber glass or aluminum alloy).

The theoretical work concerns:

(1) development of an analytical model for describing the restraining mechanisms of the armor and for prediction of ballistic limits

(2) checkout and use of a simple computer code for obtaining stress fields in brittle facing plates and projectiles caused by impact at normal incidence.

The experimental work concerns:

(1) the use of high-speed photography and flash X-ray techniques for specific investigations such as observing fracture conoids in facing plates

(2) demonstrating that stresses in ceramic facing plates can be measured by manganin stress gages.

ACKNOWLEDGMENTS

The author is indebted to J. D. Colton for supervising the manganin stress gage experiments, to W. A. Zietzke for carrying out the entire experimental program, to B. P. Bain for computer programming, to G. S. Cartwright and G. R. Greenfield for framing camera operation, to K. E. Nelson for flash X-ray unit operation, to R. E. Ray and R. L. Talbert for electronic support, and to J. W. Engle, Jr., for photographic services.

CONTENTS

ABSTRACT			iii
ACKNOWLEDGMENTS			v
LIST OF ILLUSTRATIONS			ix
LIST OF TABLES			xi
I	INTRODUCTION AND SUMMARY		1
	A.	Introduction	1
	B.	General Conclusions	2
II	RESTRAINING ACTION OF A FLEXIBLE BACKING LAYER		5
	A.	Introduction	5
	B.	Analytical Model	5
	C.	Armor Weight Optimization Using the Analytical Model	7
	D.	Conclusions	9
III	STRESS WAVES IN A PROJECTILE AND BRITTLE FACING PLATE		11
	A.	Introduction	11
	B.	Theoretical Results	12
	C.	Conclusions	13
IV	EXPERIMENTAL OBSERVATIONS OF PROJECTILE-ARMOR IMPACT		19
	A.	Introduction	19
	B.	Discussion of Experimental Results	19
	C.	Conclusions	23

CONTENTS (Concluded)

V	IMPACT STRESSES IN ALUMINUM OXIDE		41
	A.	Introduction	41
	B.	Description of Experiments	41
	C.	Experimental Results	42
	D.	Conclusions	43
REFERENCES			45
APPENDIX A	IMPULSIVE MOTION OF AN ELASTIC MEMBRANE		47
APPENDIX B	PRESSURE MEASUREMENTS WITH MANGANIN GAGES		51

ILLUSTRATIONS

Figure		Page
1	Description of Analytical Model	6
2	Predictions of the Analytical Model	8
3	Principal Planes When Principal Tensile Stress Exceeds 7 kbar	14
4	Hoop Stress Locations When Tensile Stress Exceeds 7 kbar	15
5	Principal Planes When Principal Tensile Stress Exceeds 7 kbar, Yield Criterion Included	16
6	Hoop Stress Locations When Tensile Stress Exceeds 7 kbar, Yield Criterion Included	17
7	Impact at 1800 ft/sec of 0.458-Caliber Projectile and 0.233-Inch-Thick Ceramic Tile	25
8	Impact at 1800 ft/sec of 0.458-Caliber Projectile and 0.375-Inch-Thick Ceramic Tile	26
9	Impact at 1800 ft/sec of 0.458-Caliber Projectile and 0.600-Inch-Thick Ceramic Tile	27
10	Impact at 1800 ft sec of 0.458-Caliber Projectile and 0.375-Inch-Thick Ceramic Tile Angle of Incidence 45°	28
11	Impact at 2400 ft/sec of 0.30-Caliber Projectile and 0.233-Inch-Thick Ceramic Tile	29
12	Impact at 2800 ft/sec of 0.30-Caliber Projectile and 0.233-Inch-Thick Ceramic Tile	30
13	Impact at 2400 ft sec of 0.30-Caliber Projectile and 0.600-Inch-Thick Ceramic Tile	31
14	Impact at 2800 ft/sec of 0.30-Caliber Projectile and 0.600-Inch-Thick Ceramic Tile	32

ILLUSTRATIONS (Continued)

Figure		Page
15	Impact at 2400 ft/sec of 0.30-Caliber Projectile and 0.600-Inch-Thick Ceramic Tile. Angle of Incidence 45°	33
16	Oblique Rear View of 0.600-Inch-Thick Ceramic Tile Impacted at 2400 ft sec by 0.30-Caliber Projectile	34
17	Oblique Rear View of 0.30-Caliber Standard AP Projectile Impacting 0.43-Inch-Thick Boron Carbide Tile at 2400 ft/sec. 8.33 μsec Between Frames	36
18	Impact at 2400 ft/sec of 0.30-Caliber Projectile and Composite Armor. 0.34-Inch-Thick Aluminum Oxide Bonded to 0.25-Inch-Thick Fiber Glass	37
19	Impact at 2400 ft/sec of 0.30-Caliber Projectile and Composite Armor. 0.34-Inch-Thick Aluminum Oxide Bonded to 0.25-Inch-Thick 6061-T6 Aluminum	38
20	Conoidal Fracture Formation in a 1-1/4-Inch-Thick Glass Block Impacted at 350 ft/sec by an 0.30-Caliber Round-Nose Projectile of Mild Steel	39
21	Schematic Experimental Arrangements	42
22	Manganin Gage Records	44
A-1	Stretched Circular Membrane	50
B-1	Manganin-Ceramic Gage	54
B-2	Experimental Configuration for Flying Plates	55
B-3	Experimental Configuration for Flat-Nosed Projectiles	56
B-4	Electrical Circuitry for Displaying Voltage and Voltage Change (V and ΔV)	57

TABLES

Table		Page
I	Main Experimental Parameters	24
II	Peak Stresses (kbar) in Aluminum Oxide	43

I INTRODUCTION AND SUMMARY

A. Introduction

This report* describes a continuing experimental and theoretical investigation of the interaction of hard steel projectiles and lightweight composite armor. The armor of interest consists of a very hard, relatively inflexible, facing plate of ceramic (aluminum oxide) bonded to a flexible backing plate (fiber glass or 6061-T6 aluminum alloy). The ultimate objectives of this investigation are to describe the mechanisms of interaction and to determine their dependence upon material and geometric properties.

This work is a continuation of earlier work carried out at Stanford Research Institute.[1] Based on experimental and theoretical results reported in Ref. 1 and results of this study, a description of the sequence of events that occurs when an ogive-shaped hard steel projectile strikes composite armor with a ceramic facing plate backed by a flexible plate is as follows:

1. The tip of the projectile is shattered into many small fragments (1 mm). Shattering occurs because radial and circumferential tensile stresses greatly exceeding the fracture stress are immediately set up at the tip. These small fragments move radially across the surface of the ceramic face at about twice the projectile velocity. (These fragments carry off about 7% of the kinetic energy in the case of the all-steel projectiles used in the experiments.) Shattering also causes an increase in the projectile-plate contact area (due to the ogive shape) and consequently produces a spreading of the load on the plate.

2. Comminution and fine cracking of the ceramic facing material spreads from the impact zone because of an expanding field of large tensile stresses; this field follows a compressive wave front. Ceramic powder is ejected from around the projectile impact area. The volume occupied by fine cracking is conoidal in shape.

*Part I is Reference 1.

3. Cracking at the face opposite to the impact zone develops rapidly. Initially, this cracking is predominantly radial, because the expanding tensile stress field has large circumferential stress components moving ahead of other stress components. The density of cracking decreases away from the impact zone because of geometrical attenuation of the tensile stress field and, apart from some radial cracks, is largely confined to a conoidal-shaped volume.

4. The projectile and broken ceramic exert pressure on the flexible backing over a circular area with a diameter a little larger than the diameter of the fracture conoid base. The backing absorbs energy initially by bending and ultimately by stretching.

The extension of the work of Ref. 1 reported here concerns:

- Creation of a simple analytical model to describe the restraining mechanism of composite armor and to predict ballistic limits (Section II).
- Checking and extension of a computer program for describing stress waves generated in projectiles and facing plates by impact (Section III).
- Further experimentation with a high-speed camera and an X-ray unit to describe projectile-armor interaction (Section IV).
- Study of the use of manganin stress gages to establish stress profiles in ceramic facing plates (Section V).

B. General Conclusions

A simple analytical model has been formulated to describe the restraining action of composite armor. Experimental observations and results are used in the formulation but it may be possible in the future to replace this portion with a simple theoretical description. Predictions of ballistic limits are reasonable enough to justify pursuing this approach in armor research.

The computer program of Ref. 1 that describes elastic stress waves in projectiles and hard facing plates has been checked in special impact cases by comparison with two other programs. The program has also been extended to include a yield condition. The stress distributions are compatible with observed fracture patterns. To complete

the description, research is necessary to establish a fracture criterion for inclusion in the computer program.

Experiments with ceramic plates have provided evidence that if the plate is thick enough an integral fracture conoid is punched out by the projectile. Low impact velocity experiments with glass blocks and mild steel projectiles also show the formation of an integral fracture conoid. This conoid shape is independent of the impact velocity and is probably a strong function of the plate sound velocity. Thus, armor experiments can be designed using glass facing plates to study breakup of opaque ceramic facing plates.

Use of manganin stress gages is feasible for establishing compressive wave fronts in ceramic facing plates. The results are invaluable for correlation with theoretical predictions.

II RESTRAINING ACTION OF A FLEXIBLE BACKING LAYER

A. Introduction

When a projectile strikes the hard ceramic facing of composite armor, most of the momentum is spread over a circular area, the diameter of which is dependent on the mechanical and geometrical properties of the projectile and ceramic facing. The fiber glass or aluminum alloy backing that is bonded to the ceramic is a flexible layer that bends and stretches to absorb the kinetic energy of the projectile and broken ceramic within the circular area. Experimental observations indicate that for much of the motion the backing remains bonded to the ceramic facing outside the circular area thus confining most of the kinetic energy absorption to the backing within the circular area. Consequently, the backing can be analyzed as a circular membrane or plate fixed at the circular boundary and having an initial mass and velocity distribution.

B. Analytical Model

A simple model for describing the action of two-layer composite armor is illustrated in Fig. 1. The projectile is idealized to a short cylindrical rod with a diameter equal to that of the armor-piercing core. The diameter of the circular area of the backing over which the momentum is spread is taken as the base diameter of the fracture conoid in the ceramic facing. Finally, the backing is assumed to respond as a circular membrane. The mass of the membrane is approximated by a uniform mass that is the average over the circular area of the sum of the masses of the projectile, ceramic conoid (approximately conical), and the backing layer within the circle. The velocity distribution is associated with the fundamental mode of vibration of the circular membrane with a peak value determined by momentum conservation.

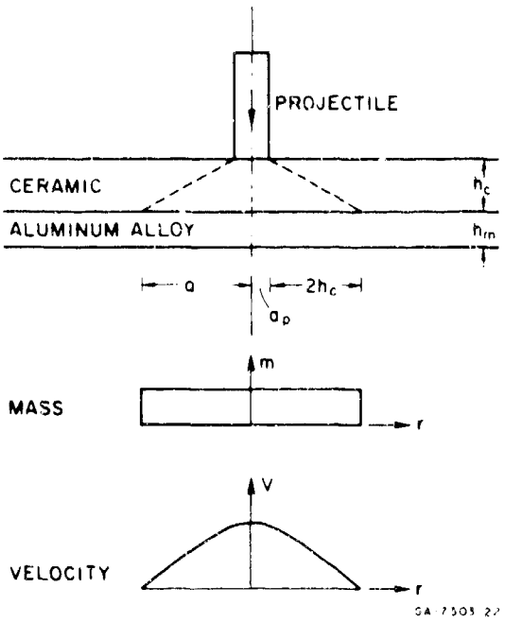

FIGURE 1 DESCRIPTION OF ANALYTICAL MODEL

The analysis of the membrane is contained in Appendix A. One of the results obtained is the following simple formula for the maximum strain ε_r:

$$\varepsilon_r = 1.82 \cdot f(a) \cdot K/S \qquad (1)$$

where $f(a)$ is a simple ratio, K is the kinetic energy of the projectile before impact, and S is the constant tension in the membrane. In terms of the projectile mass M_p, projectile velocity V_p, ceramic mass per unit area m_c, backing mass per unit area m_m, conoid base radius a, backing material yield stress σ, and backing thickness h_m,

$$K = M_p V_p^2 \, 2$$

$$S = \pi h_m$$

$$f(a) = M_p \left[M_p + (m_c + m_m) \pi a^2 \right] \pi a^2$$

An approximation to experimental results reported here for aluminum oxide* is the conoid base radius $a = a_p + 2h_c$, where a_p is the projectile radius and h_c is the ceramic thickness (see Fig. 1). The behavior of the backing material is taken as rigid plastic, which is reasonable for 6061-T6 aluminum alloy, a commonly used material in composite armor.

By using a maximum strain failure criterion in the backing material, formula (1) predicts a ballistic limit

$$V_p = \left[\varepsilon_r S \sigma / 0.91 \, M_p f(a) \right]^{1/2} \qquad (2)$$

C. Armor Weight Optimization Using the Analytical Model

The simple analytical model can be used to minimize the areal density of a ceramic-aluminum armor. This optimization is now described for a standard 0.30-caliber AP (Armor Piercing) projectile with a mass $M_p = 10$ g. The radius of the idealized cylindrical projectile is taken as the radius of the core of the AP projectile, that is, $a_p = 0.125$ inch. The fracture strain and yield stress for the aluminum alloy backing material (6061-T6) are taken as $\varepsilon_r = 0.15$ and $\sigma = 3 \times 10^9$ dynes/cm^2 (44,000 lb/in^2). The remaining properties required, the densities of the ceramic and aluminum, are $\rho_m = 2.7$ g/cm^3 and $\rho_c = 3.6$ g cm^3.

For a given backing or membrane thickness h_m, a projectile velocity V_p producing strain $\varepsilon_r = 0.15$ in the aluminum is predicted by formula (2) for each chosen value of ceramic thickness h_c. Thus curves of the type shown in Fig. 2a are readily obtained. Figure 2a shows three curves corresponding to membrane thicknesses of $h_m = 1/8$, 1/4, and 3/8 inch. If the projectile velocity is 3000 ft/sec the

*Aluminum oxide AD94, manufactured by Coors Porcelain, Golden, Colorado.

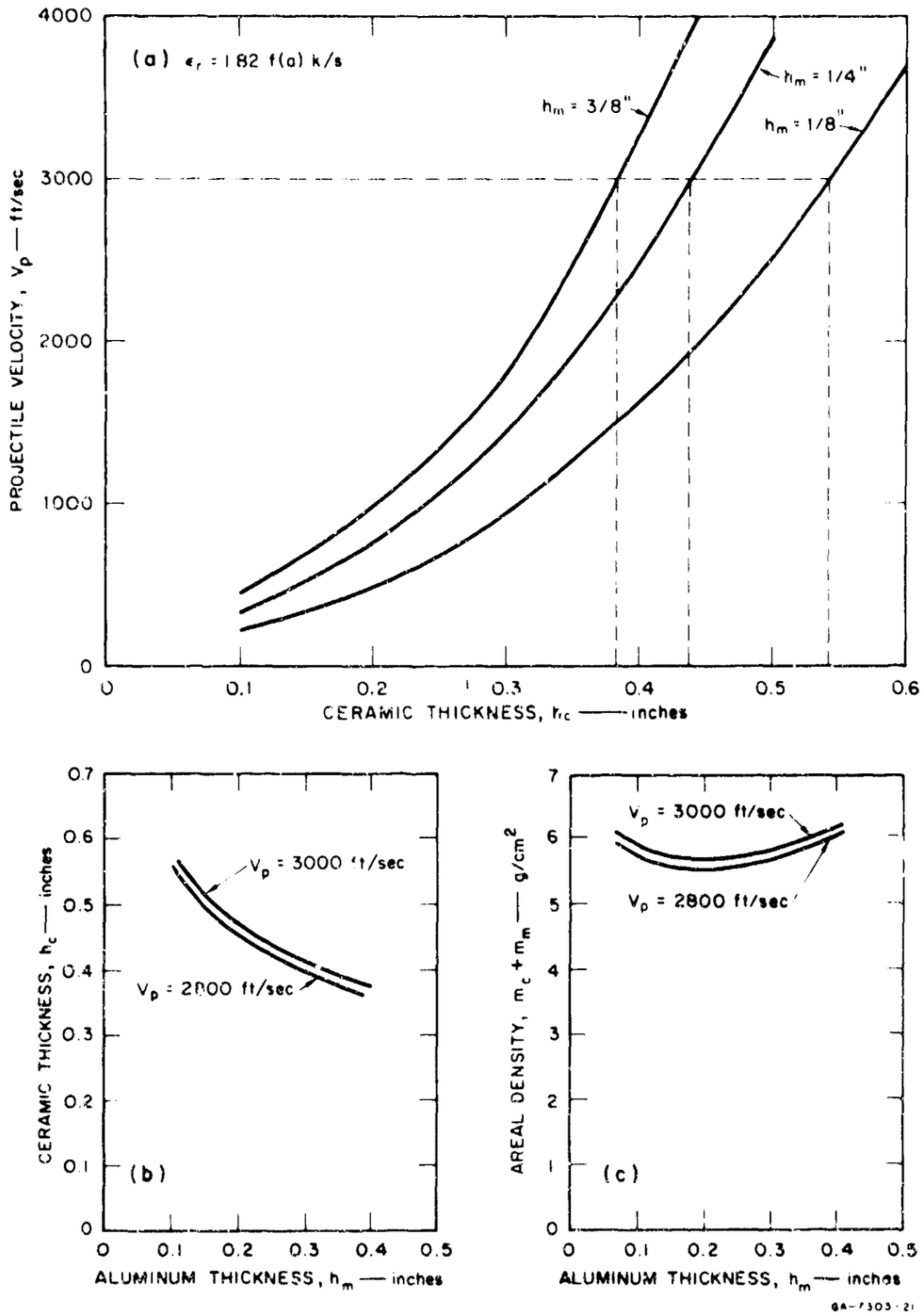

FIGURE 2 PREDICTIONS OF THE ANALYTICAL MODEL

required ceramic thicknesses accompanying these membrane thicknesses are h_c = 0.545, 0.44, and 0.385 inch, as indicated in Fig. 2a by the vertical dashed lines. Figure 2b shows a curve through these ceramic and aluminum thickness points. Plotting instead the areal density $m_c + m_m$ of the armor against the aluminum thickness results in the upper curve shown in Fig. 2c.

The upper curve in Fig. 2c shows that the predicted minimum areal density required to defeat an 0.30-caliber AP projectile impacting at 3000 ft sec is about 5.7 g cm^2 (11.3 lb/ft^2), the thicknesses of the ceramic and aluminum being about 0.47 and 0.20 inch. For an impact velocity of 2800 ft/sec these quantities are 5.5 g/cm^2 (11.0 lb/ft^2), 0.45 inch, and 0.20 inch. Ballistic test results show that the ballistic limit is 2850 ± 50 ft sec for ceramic and aluminum thicknesses of 0.34 and 0.25 inch giving an areal density of 4.82 g cm^2 (9.8 lb/ft^2). Thus for the example of composite armor consisting of aluminum oxide facing and 6061-T6 aluminum alloy backing being impacted by an 0.30-caliber AP projectile, the simple analytical model provides approximate thicknesses for minimum weight for each projectile velocity.

D. Conclusions

The above example demonstrates that a simple analytical model can be useful for approximate ballistic limit predictions. It is always possible to refine a model but only at the expense of simplicity. Future work should concentrate on generating possible alternative models, finding the degree of refinement attainable before simplicity is forfeited, and incorporating newly acquired theory whenever it can simply replace empirical relations. The latter improvement applies to the determination of the ceramic cone size in the model described above. The construction of analytical models should be guided by experimental observations and numerical solutions of impact problems, and the predictions correlated with experimental results. Once confidence has been established in a model it may be used for predictions.

III STRES WAVES IN A PROJECTILE AND BRITTLE FACING PLATE

A. Introduction

In Ref. 1 a numerical scheme[2] was adopted for solving finite-difference analogues of the elasticity equations governing stress wave propagation in a steel projectile and a ceramic layer caused by axial impact (projectile idealized as a circular cylinder). Because analytic solutions for this impact problem are not available the above numerical scheme was tested in this project by correlating results with the results stemming from a different numerical scheme.[3,4] Agreement between the results of the two computer programs was found to be satisfactory. Another check on the computer program was performed by comparison with results from SRI PUFF 2 code[5] for the special case of one-dimensional plane strain waves caused by the impact of two plates. Again, agreement was satisfactory.

Two sets of results are presented below. In the first set (Figs. 3 and 4), principal planes within the projectile and facing plate are indicated wherever the maximum tensile stress exceeds about 7 kbar. The orientations of these planes indicate the probable fracture planes. The results given in Fig. 3 and 4 are refined and extended versions of results already reported in Ref. 1. In the second set of results (Figs. 5 and 6), a von Mises yield criterion has been employed, which has the effect of limiting the distortional component of stress (as opposed to the hydrostatic component of stress) acting on each material element. After a search of the literature on fracture it was decided that information was insufficient to incorporate a meaningful fracture criterion. It is believed that this situation can be remedied with an experimental program with ceramics that establishes spall thresholds from reflection of uniaxial strain waves generated by plate impact.

B. Theoretical Results

The data used in the computations of stress fields caused by rod-plate impact at 2400 ft/sec are:

	Plate	Rod	Units
Material	Al oxide (AD94)	steel	
Density	3.6	7.8	g/cm^3
Young's modulus	39.6×10^6	30×10^6	lb/in^2
Shear modulus	15.8×10^6	11.6×10^6	lb/in^2
Bulk modulus	26.4×10^6	23.8×10^6	lb/in^2
Poisson's ratio	0.25	0.29	
Dilatational velocity	31,300	19.300	ft/sec
Yield stress (compressive)	1150×10^3	100×10^3	lb/in^2
Yield stress (tensile)	43.5×10^3	100×10^3	lb/in^2
Thickness	0.34		in
Diameter		0.24	in

Figures 3 and 4 correspond to elastic material behavior. Each of the nine diagrams in each figure displays a meridional plane at a certain time and the lines and dots indicate where tensile stress components have exceeded 7 kbar. These stress components act perpendicularly to the lines shown in Fig. 3 and perpendicularly to the meridional plane in Fig. 4. Thus Fig. 3 shows the probable characters of axisymmetric fracture patterns whereas Fig. 4 indicates where radial cracking is likely (but not of course how many radial cracks will occur).

Figures 5 and 6 correspond to elastic-perfectly plastic material behavior, and it is seen by comparison with Figs. 3 and 4 that introducing a yield condition has the effect of reducing considerably the region where fracture is likely.

C. Conclusions

A simple computer program for solving the axisymmetric equations of elasticity, with or without a yield criterion, predicts stress fields in brittle facing plates and projectiles compatible with observed fracture patterns. The program is of value for:

1. Correlation of predictions with experimental results.
2. Providing a basis for including a fracture criterion once one has been established.
3. Guiding the formulation of a simple model for the facing plate mechanism.

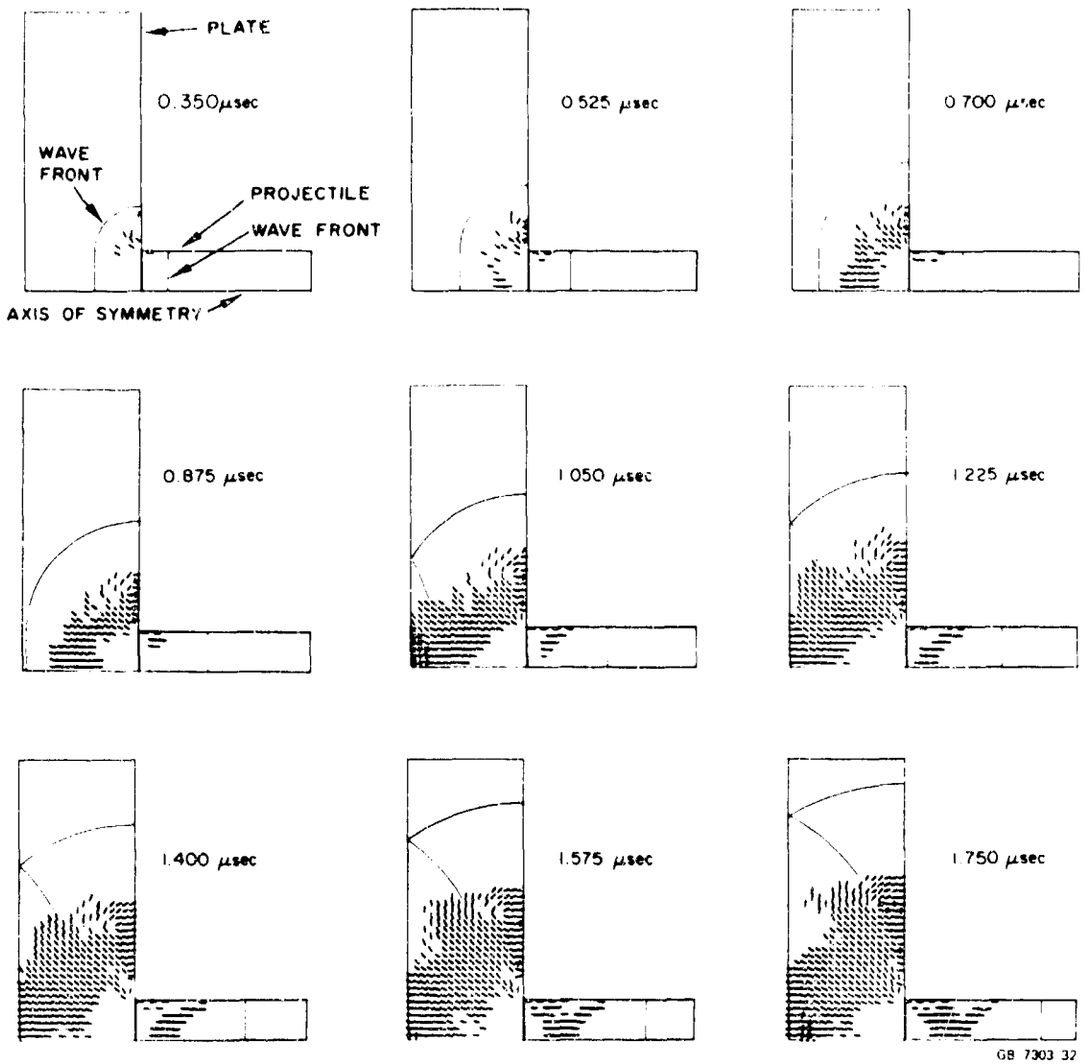

FIGURE 3 PRINCIPAL PLANES WHEN PRINCIPAL TENSILE STRESS EXCEEDS 7 kbar

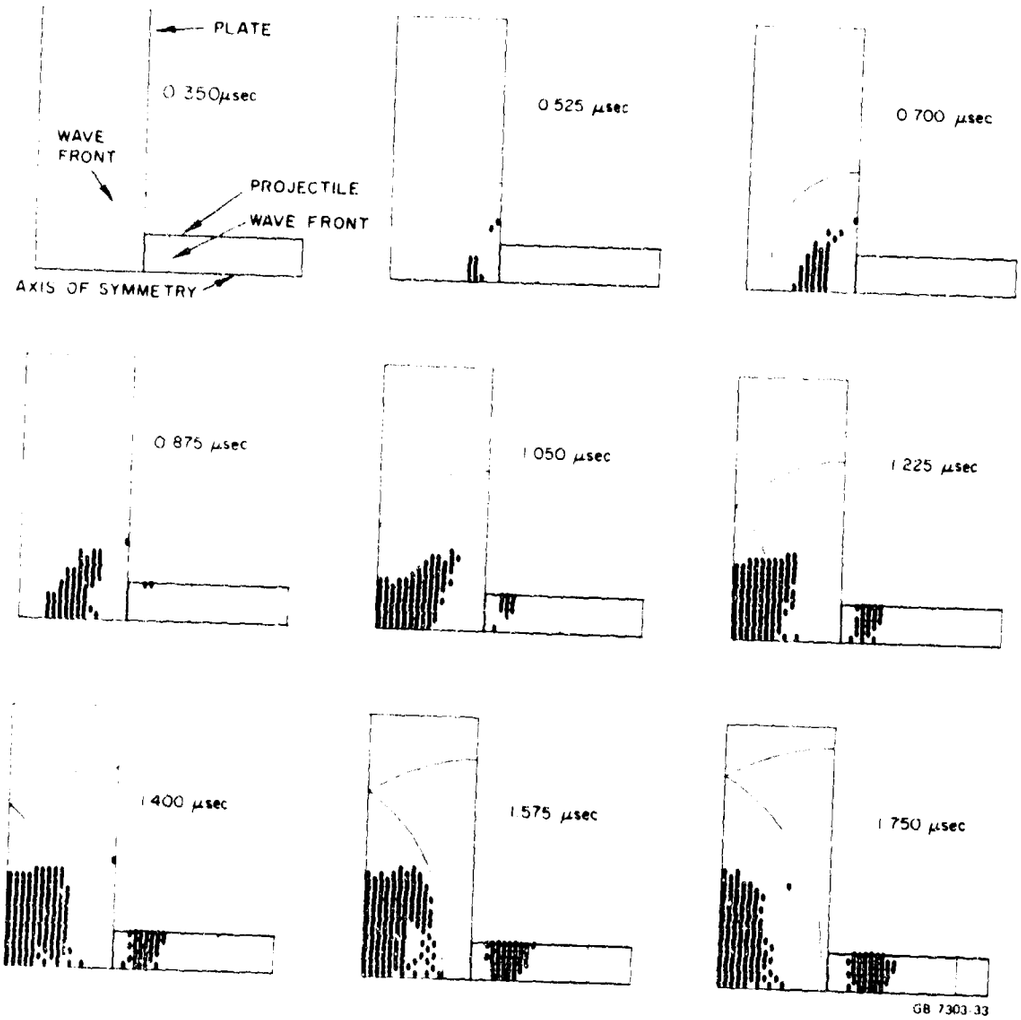

FIGURE 4 HOOP STRESS LOCATIONS WHEN TENSILE STRESS EXCEEDS 7 kbar

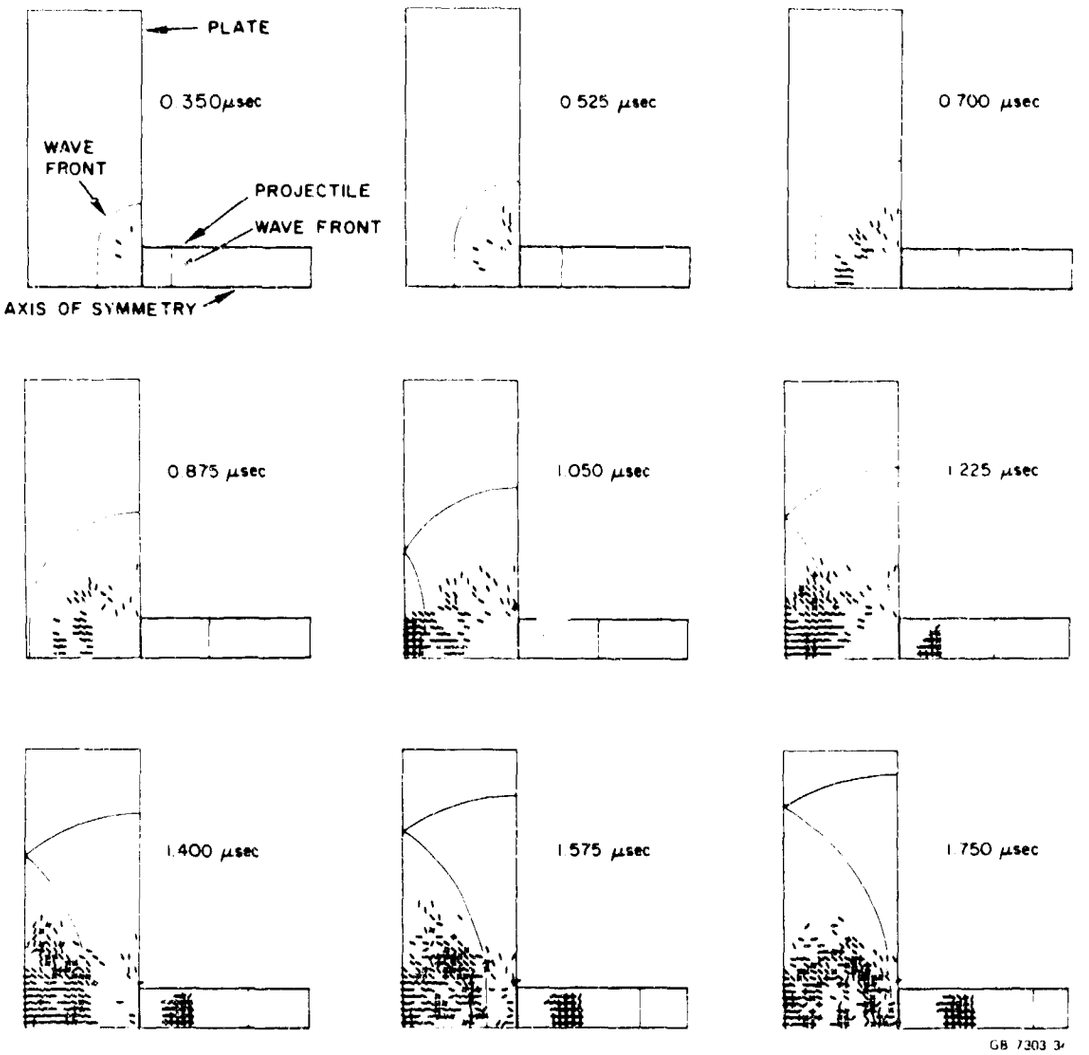

FIGURE 5 PRINCIPAL PLANES WHEN PRINCIPAL TENSILE STRESS EXCEEDS 7 kbar
Yield Criterion Included

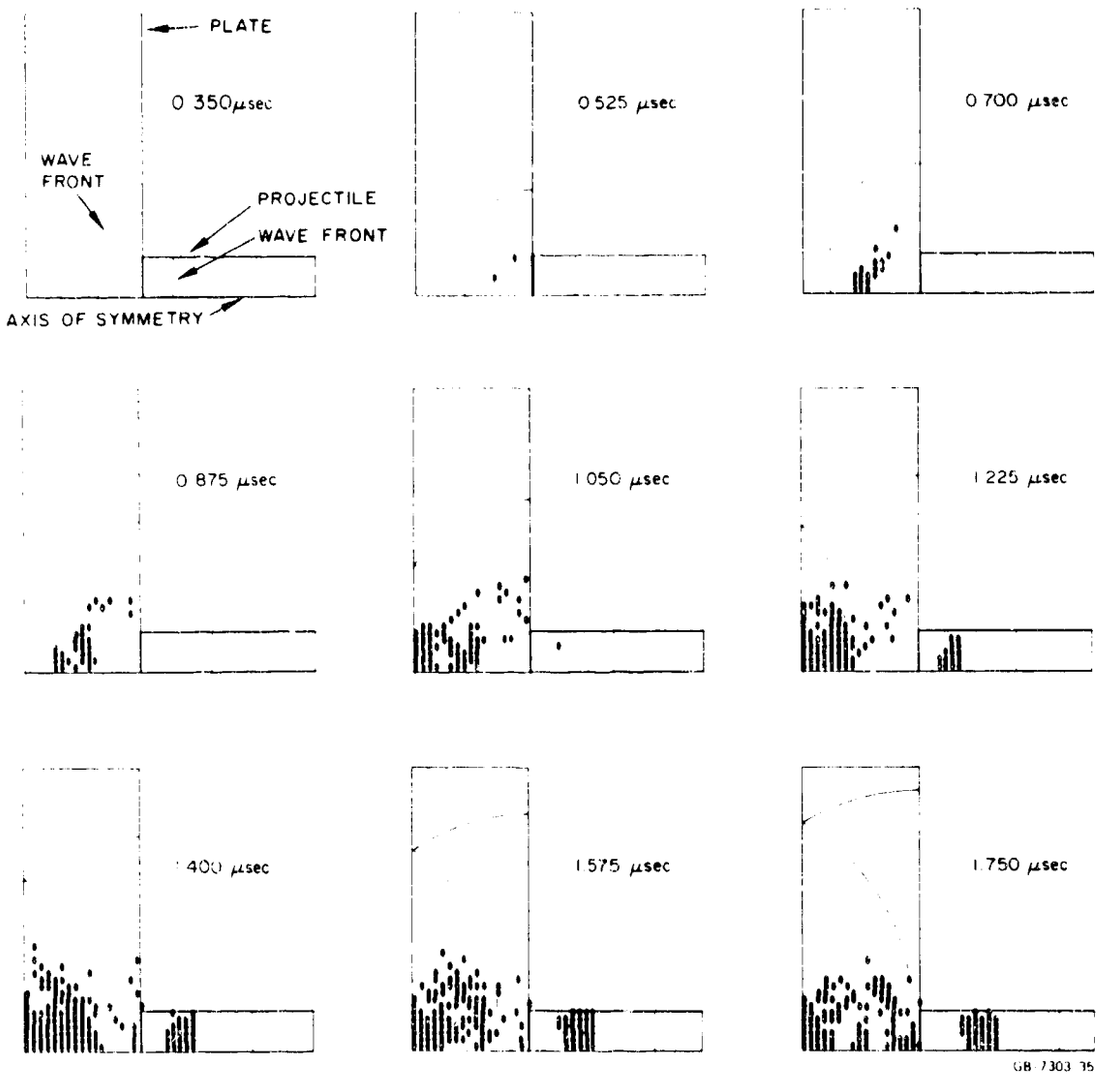

FIGURE 6 HOOP STRESS LOCATIONS WHEN TENSILE STRESS EXCEEDS 7 kbar
Yield Criterion Included

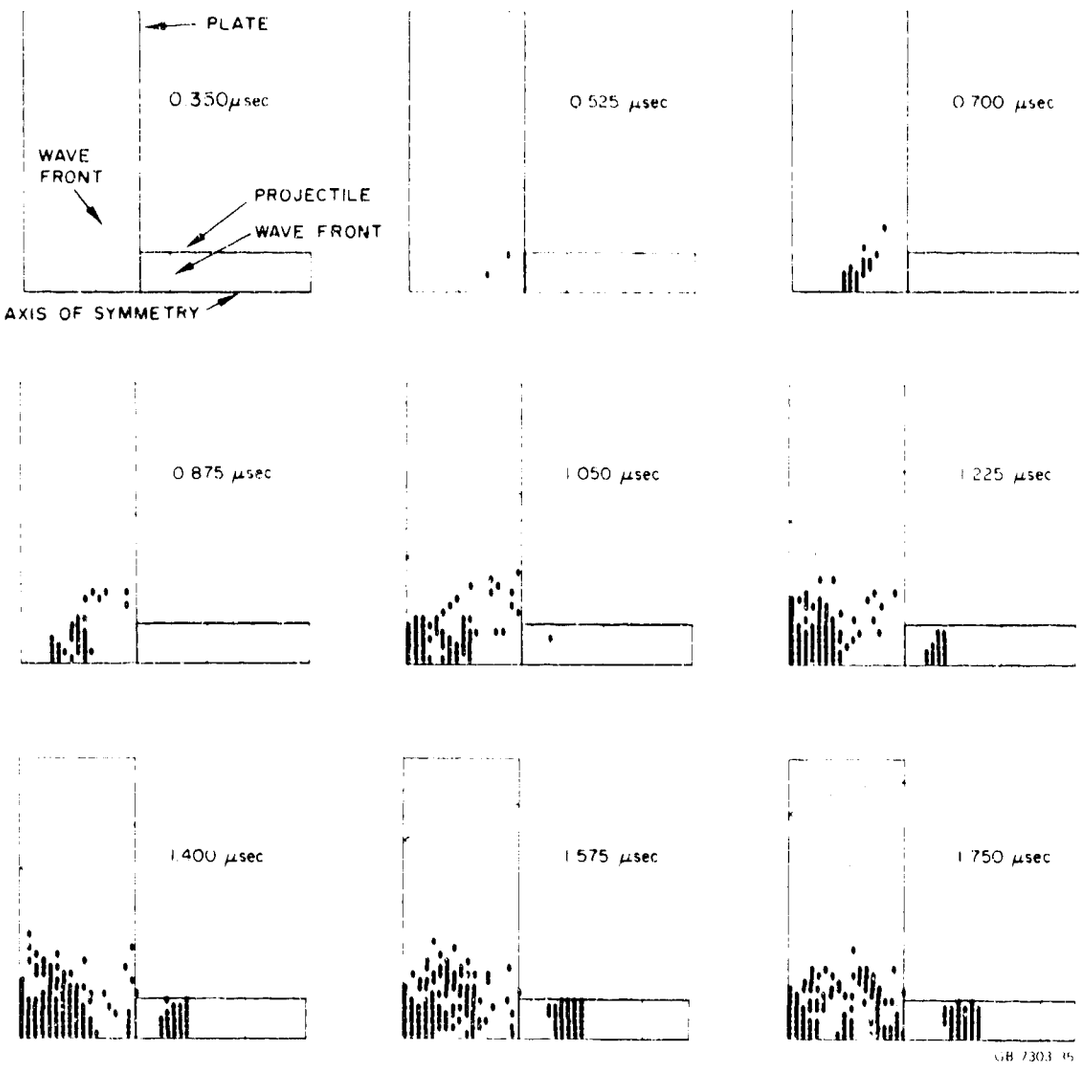

FIGURE 6 HOOP STRESS LOCATIONS WHEN TENSILE STRESS EXCEEDS 7 kbar
Yield Criterion Included

IV EXPERIMENTAL OBSERVATIONS OF PROJECTILE-ARMOR IMPACT

A. Introduction

Impact experiments were conducted with 0.30- and 0.458-caliber projectiles and target plates of aluminum oxide, boron carbide, aluminum oxide backed by fiber glass, aluminum oxide backed by 6061-T6 aluminum alloy, and glass. The impact events were recorded by X-ray or framing camera. The objective of the experiments was to record breakup and deformation characteristics of projectiles and composite armor facing and backing plates. These characteristics not only contribute to the understanding of projectile/armor interaction but are indispensable for formulating a theoretical description of the interaction, both by simple analytical models and numerical analysis with computer codes.

The main experimental parameters are listed in Table I. Each of the figures in the following pages which show radiograph records (except for Fig. 20) consists of a sequence of from two to five events, and each event represents a different but identical experiment.

A summary of the conclusions based on the experiments listed in Table I follows the discussions.

B. Discussion of Experimental Results

Figure 7 shows an 0.458-caliber projectile impacting an 0.233-inch-thick ceramic tile at a velocity of 1800 ft/sec and at normal incidence. The impact stresses cause a shattering of the nose tip and shorten the projectile, which was originally 1-11/16 inches long by about 5/16 inch. The diameter of the breakup area of the ceramic is about 1-1/2 inches. Figure 8 is a similar sequence of events except that the tile is 0.375 inch thick. Not only has the projectile tip shattered but the remainder of the projectile has broken into two or three large pieces.

The diameter of the breakup area of the ceramic has increased to about 1-7/8 inches. A third similar sequence of events is shown in Fig. 9 with a tile 0.60 inch thick, the maximum thickness used in the experiments. The projectile has now fractured into still more pieces and has become disoriented. Based on measurements made from Fig. 9b, the diameter of the major breakup area of the ceramic has increased to about 3-3/8 inches.

Figure 10 shows a 0.458-caliber projectile impacting an 0.375-inch-thick tile at 1800 ft sec and at a 45° angle of incidence. The projectile shattering is similar to that occurring at normal incidence (Fig. 8) but a major fracture is oriented across the projectile and is caused by the asymmetrical stress distribution. Also, the tile has the effect of rotating the projectile. The area of ceramic breakup appears to be similar to that occurring for comparable impact at normal incidence, but the momentum distribution that would be applied to a backing plate, were it present, would be quite different.

Figure 11 shows a standard 0.30-caliber projectile impacting an 0.233-inch-thick tile at a velocity of 2400 ft/sec and at normal incidence. A small portion of the tip of the hard steel core has been shattered and the copper jacket has been partially removed. Based on measurements made from Fig. 11b the diameter of broken ceramic is about 1-1/2 inches. Figure 12 is a repeat of this experiment but with an impact velocity of 2800 ft/sec. More of the core tip has been removed but the diameter of the broken ceramic remains about 1-1/2 inches.

Figure 13 describes the impact when the velocity is 2400 ft/sec and the ceramic tile is 0.60 inch thick. These records are especially interesting because, as can be seen in Fig. 13c, the rear surface of the tile remains flat and parallel to the rear surface of the tile before impact over a circular area of about 1-1/2 inches in diameter. Figure 13d reveals that this portion of the tile is a fracture conoid of a height approximately equal to the tile thickness. A rough measurement of the "cone" angle is 66°. Such conoids have been observed in glass blocks struck at low impact velocity[1] suggesting a similarity between the mechanics taking part in the glass and ceramic experiments. (This

similarity is discussed further in the description of Fig. 20 below.) The jacket of the projectile is completely removed and the core is fractured. Figure 14 describes a repeat experiment except for the impact velocity which is 2800 ft/sec. Figure 14b shows a rear surface displacement similar to that in Fig. 13c. The conoid is not as well preserved (Fig. 14c) due to more extensive fracture. The sizes of the ceramic fracture regions are comparable. The fracture conoid assumed in the analytical model is shown in Fig. 13c.

Figure 15 shows the oblique impact at 2400 ft/sec of an 0.30-caliber projectile and a ceramic tile 0.60 inch thick, the angle of incidence being 45°. The projectile is rotated by the tile and the emergence of a fracture conoid can be seen in Fig. 15c.

The experiment recorded by Fig. 13 was repeated before a Beckman and Whitley 189 framing camera. The underside of the 0.60-inch-thick tile was sprayed black to form a contrast with the white aluminum oxide, so that cracks could be seen more clearly. Figure 16 is the framing camera record showing the breaking of the tile as viewed from an angle of 10° to the rear surface. Initially a circular crack forms along with about 16 radial cracks outside the circle. Later another concentric circular crack of larger diameter appears. The region inside the inner circular crack is the base of the fracture conoid. In the annular region are wedges of ceramic connecting the base of the conoid with the relatively motionless outer portion of the tile. During the recording period the conoid base moves parallel to itself while the wedges rotate about the outer circle. This motion corresponds to the radiograph record (Figs. 13c and 13d) of the identical experiment.

Figure 17 is a framing camera record showing the breakup of an 0.45-inch-thick boron carbide tile as viewed from an angle of 10° to the rear surface. The rear surface was sprayed white to form a contrast with the black boron carbide. The tile was impacted at normal incidence by an 0.30-caliber projectile with a velocity of 2400 ft/sec. It is seen that the main breakup is confined to the region within a circle about 1-1/8 inches in diameter. Failure outside this circular region consists of radial cracks extending to the edge of the plate. Figure 17 shows that the breakup mechanism is similar to that of aluminum oxide.[1]

Figure 18 shows the deformation of an 0.25-inch-thick backing plate of fiber glass, attached to an 0.34-inch-thick aluminum oxide facing plate, caused by impact at 2400 ft/sec with an 0.30-caliber projectile. Initially the re training region of the backing is confined to the circular region corresponding to the base circle of the conical fracture region of the facing. Because of the ultimate radial spreading of bond failure the circular region of backing material increases and allows an increasing quantity of backing material to be stretched and consequently to absorb kinetic energy. Provided the backing is not separated from the facing over an entire panel and provided reasonably large deflections are permissible, this is a good stopping mechanism.

Figure 19 shows the deformation of an 0.25-inch-thick backing plate of 6061-T6 aluminum alloy, attached to an 0.34-inch-thick aluminum oxide facing plate, caused by impact at 2400 ft/sec with an 0.30-caliber projectile. Most of the deformation is concentrated within a circular region corresponding the base circle of the fracture conoid in the facing. Inside this circular region plastic membrane stretching is the principal energy absorbing mechanism. Outside this circular region the backing plate displays the opposite curvature and deformations small enough to regard plastic bending as a significant energy absorbing mechanism. The radius a assumed in the analytical model is shown.

Figure 20 shows the development of a fracture conoid within a 1-1/4-inch-thick glass block caused by impact at 350 ft/sec with an 0.30-caliber round-nose projectile of 1015 steel. The angle of the average cone approximating the conoid is about 50°; this compares with the ceramic cone angle of about 66° from Fig. 13. This experiment and earlier work[1] show that a transparent brittle material such as glass can be used in appropriately designed experiments to acquire qualitative information on breakup of opaque ceramic due to projectile impact. The steel was chosen to provide a projectile material that is softer but denser than glass. Also, the impact velocity of 350 ft/sec was arrived at through several trials to obtain comparable fracture damage in the glass and an 0.60-inch-thick ceramic tile impacted at 2400 ft/sec by an 0.30-caliber AP projectile (see Fig. 13).

C. Conclusions

From the preceding experimental results and from earlier work[1] it is concluded that:

1. The extent of projectile breakup increases with ceramic facing thickness.

2. The major breakup of the facing is confined to a conoidal region with a base circle increasing with ceramic thickness. (Experimental results form the basis for approximating the radius of this circle by $a = a_p + 2h_c$ in the formulation of the analytic model of Section II, where a_p is the projectile radius and h_c is the ceramic thickness.)

3. Clear evidence of integral conoidal fractures in ceramic has been obtained.

4. Qualitatively, boron carbide tiles break up in a manner similar to that of aluminum oxide tiles.

5. Initial deformation of a flexible backing plate occurs over a circle approximately equal to the base circle of the fracture conoid. (This information was incorporated in the analytical model of Section II.)

6. Experiments can be conducted with a brittle transparent facing material such as glass to study the interaction of opaque ceramics and projectiles.

Table I

MAIN EXPERIMENTAL PARAMETERS

TARGET				PROJECTILE			Impact Incidence	Camera Type	Fig. No.
Facing		Backing		Caliber (inch)	Velocity (ft/sec)	Weight (g)			
Material	Thickness (inch)	Material	Thickness (inch)						
Aluminum oxide[a]	0.233	None		0.458	1800	24.6	Normal	X-ray	7
Aluminum oxide	0.375	None		0.458	1800	24.6	Normal	X-ray	8
Aluminum oxide	0.60	None		0.458	1800	24.6	Normal	X-ray	9
Aluminum oxide	0.375	None		0.458	1800	24.6	45°	X-ray	10
Aluminum oxide	0.233	None		0.30	2400	10.1	Normal	X-ray	11
Aluminum oxide	0.233	None		0.30	2800	10.1	Normal	X-ray	12
Aluminum oxide	0.60	None		0.30	2400	10.1	Normal	X-ray	13
Aluminum oxide	0.60	None		0.30	2800	10.1	Normal	X-ray	14
Aluminum oxide	0.60	None		0.30	2400	10.1	45°	X-ray	15
Aluminum oxide	0.60	None		0.30	2400	10.1	Normal	Framing	16
Boron carbide[b]	0.43	None		0.30	2400	10.1	Normal	Framing	17
Aluminum oxide	0.34	Fiber glass[c]	0.25	0.30	2400	10.1	Normal	X-ray	18
Aluminum oxide	0.34	Al 6061-T6	0.25	0.30	2400	10.1	Normal	X-ray	19
Glass	1.25	None		0.30[d]	350	11.2	Normal	Framing	20

[a] Aluminum oxide AD94 tiles 5-3/4 x 5-3/4 inches, manufactured by Coors Porcelain, Golden, Colorado.

[b] Boron carbide tiles 5-3/4 x 5-3/4 inches, manufactured by Norton Co., Worcester, Massachusetts.

[c] Woven roving fiber glass 9 x 9 inches, manufactured by Russell Reinforced Plastics Corp., Linderhurst, Long Island, New York.

[d] Round-nose projectile of 1015 steel.

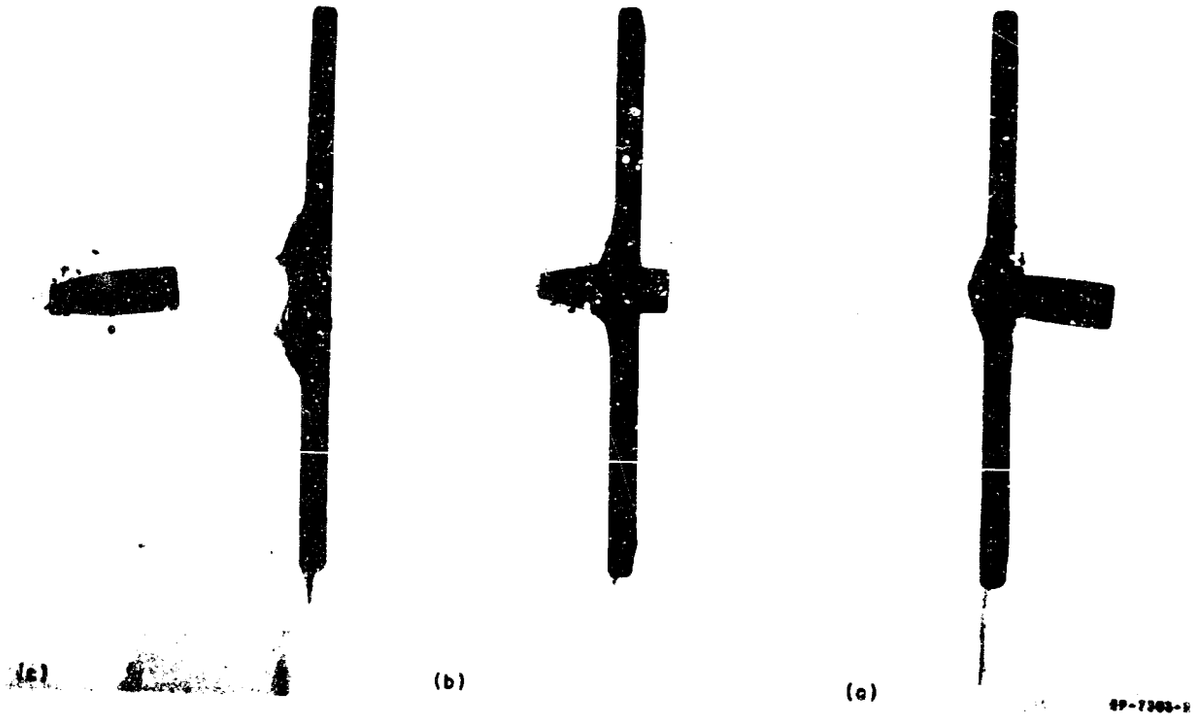

FIGURE 7 IMPACT AT 1800 FT/SEC OF 0.458-CALIBER PROJECTILE AND 0.233-INCH-THICK CERAMIC TILE

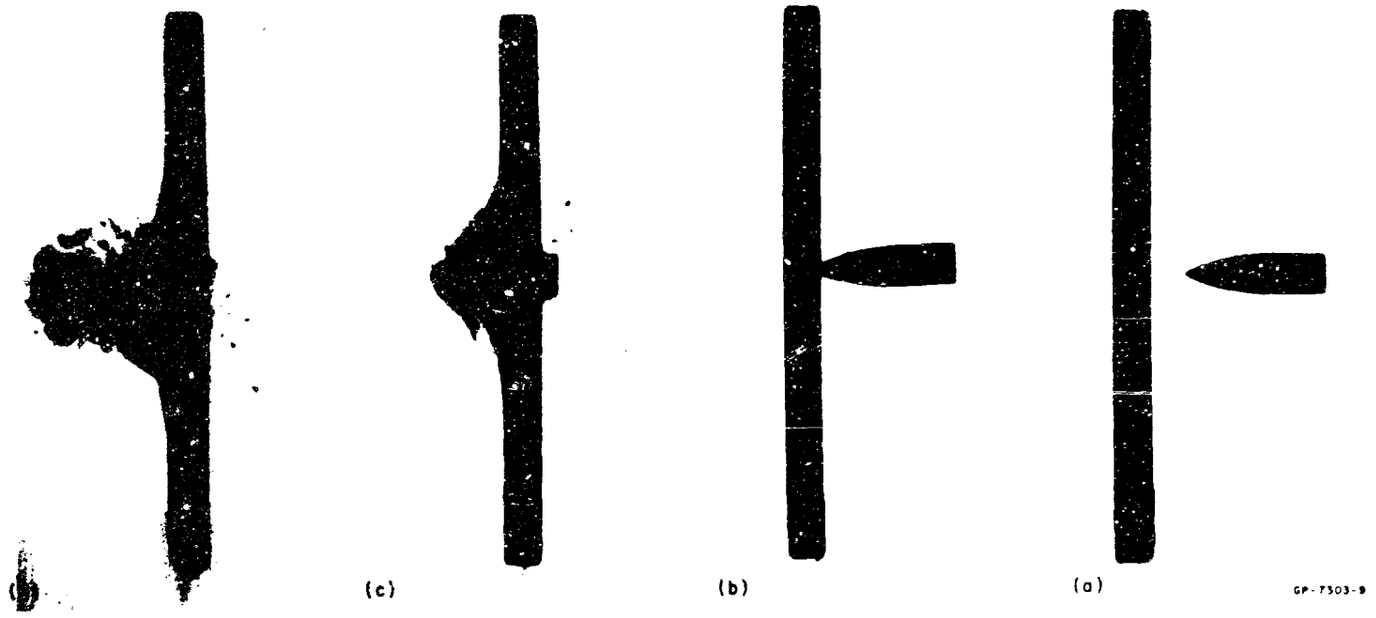

FIGURE 8 IMPACT AT 1800 FT/SEC OF 0.458-CALIBER PROJECTILE AND 0.375-INCH-THICK CERAMIC TILE

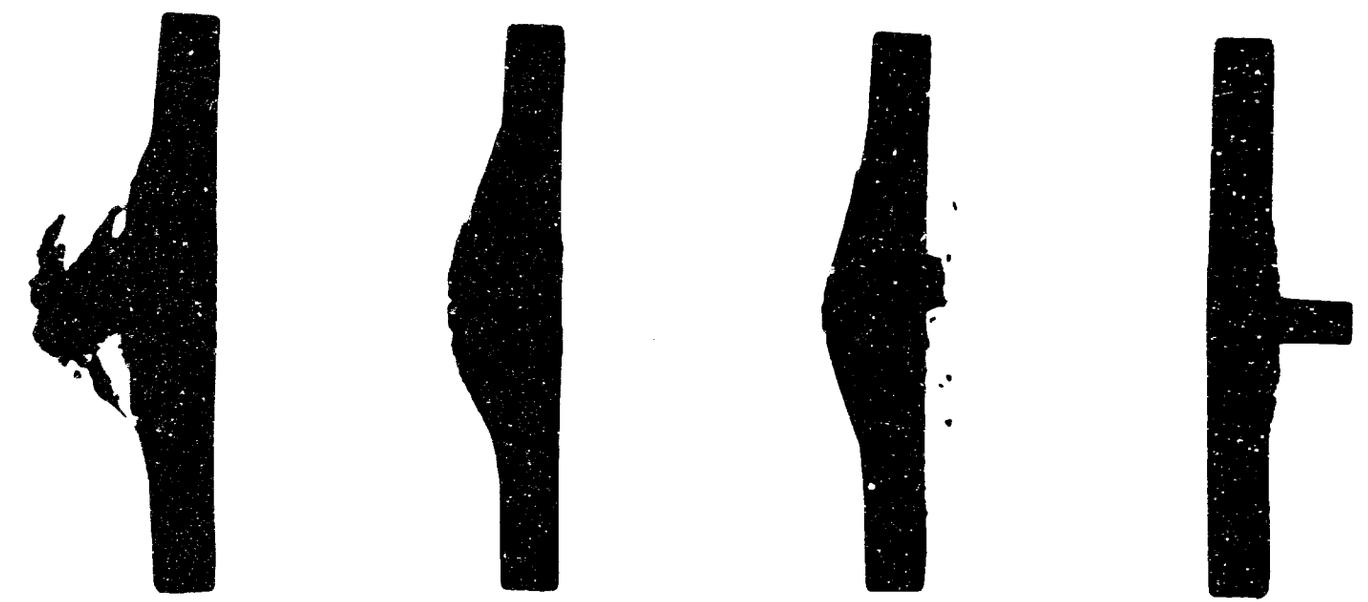

FIGURE 9 IMPACT AT 1800 FT/SEC OF 0.458-CALIBER PROJECTILE AND 0.600-INCH-THICK CERAMIC TILE

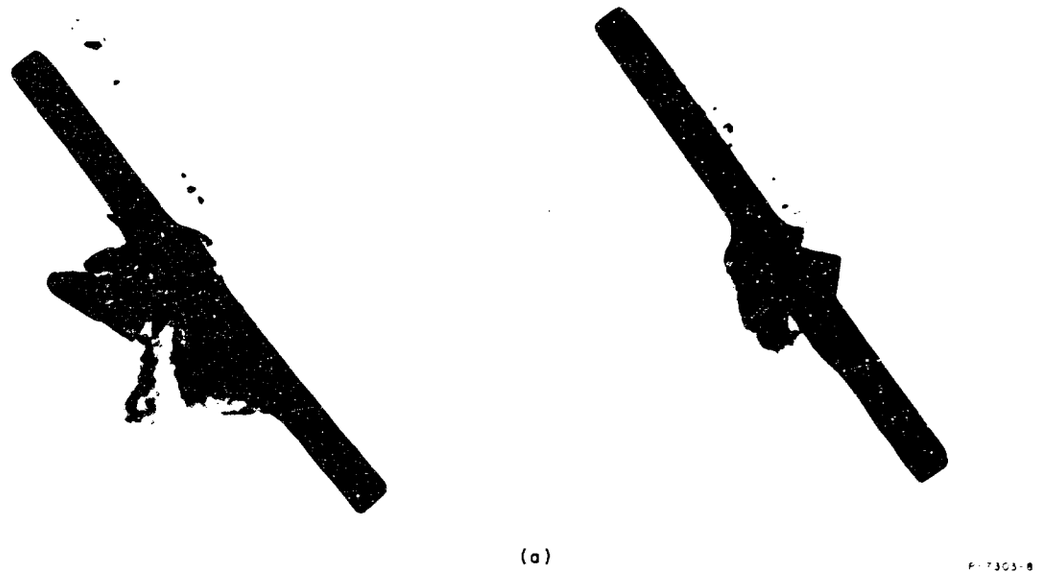

FIGURE 10 IMPACT AT 1800 FT/SEC OF 0.458-CALIBER PROJECTILE AND 0.375-INCH-THICK CERAMIC TILE Angle of Incidence 45°

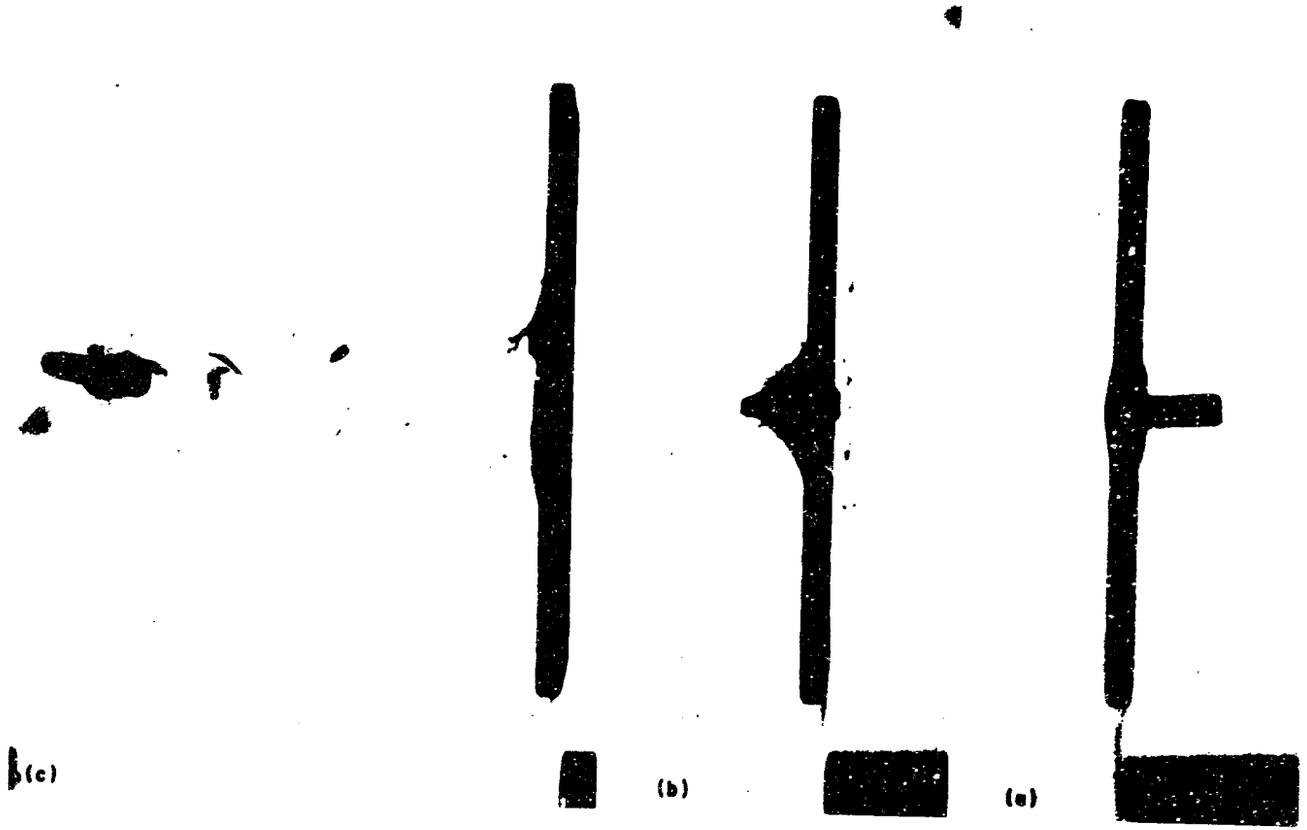

FIGURE 11 IMPACT AT 2400 FT/SEC OF 0.30-CALIBER PROJECTILE AND 0.233-INCH-THICK CERAMIC TILE

FIGURE 12 IMPACT AT 2800 FT/SEC OF 0.30-CALIBER PROJECTILE AND 0.233-INCH-THICK CERAMIC TILE

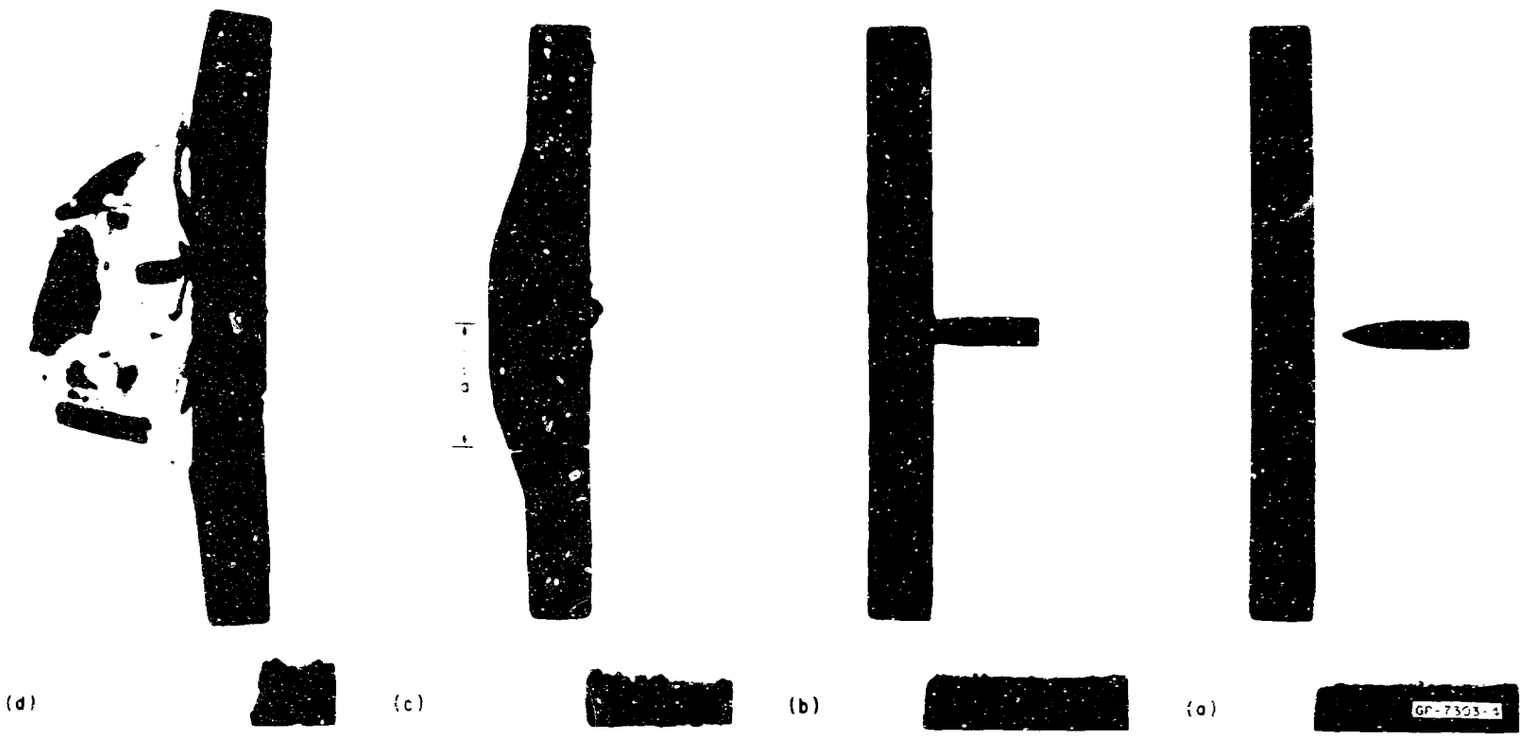

FIGURE 13 IMPACT AT 2400 FT/SEC OF 0.30-CALIBER PROJECTILE AND 0.600-INCH-THICK CERAMIC TILE

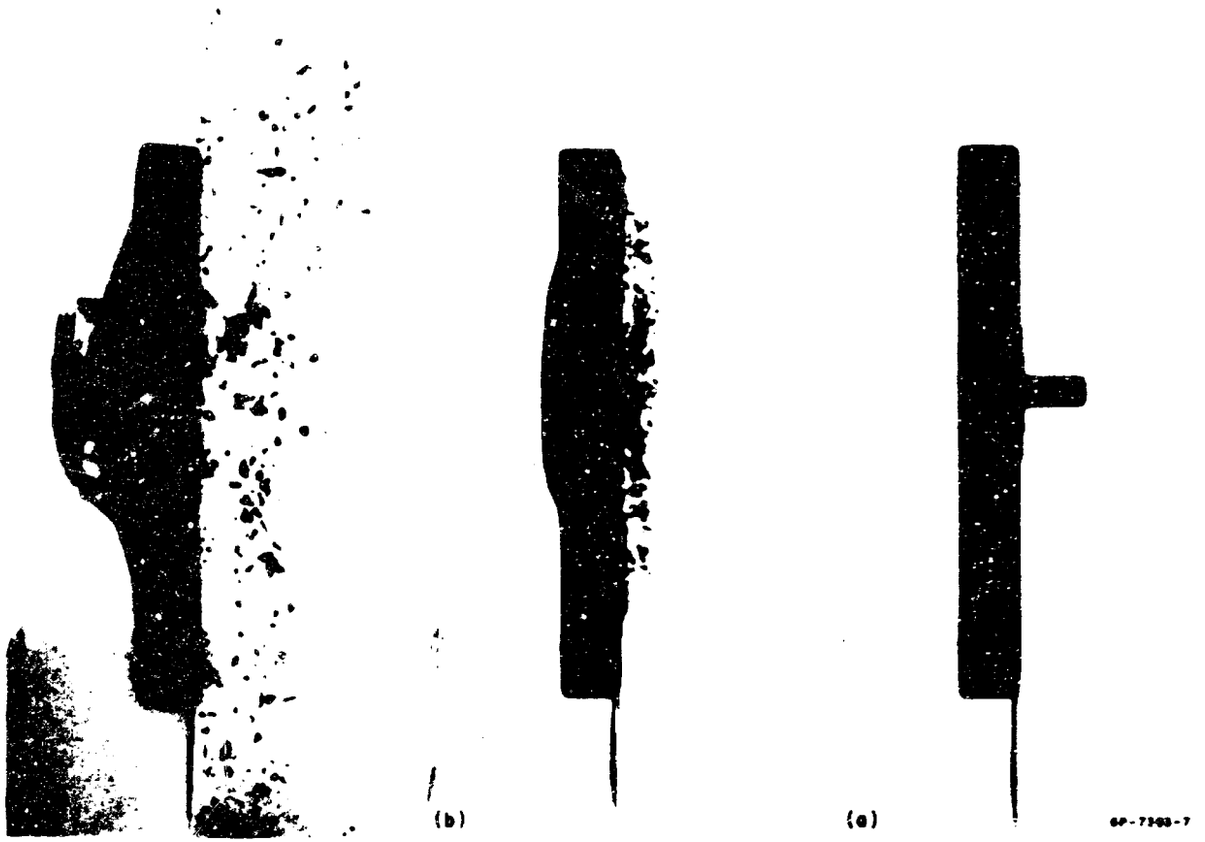

FIGURE 14 IMPACT AT 2800 FT/SEC OF 0.30-CALIBER PROJECTILE AND 0.600-INCH-THICK CERAMIC TILE

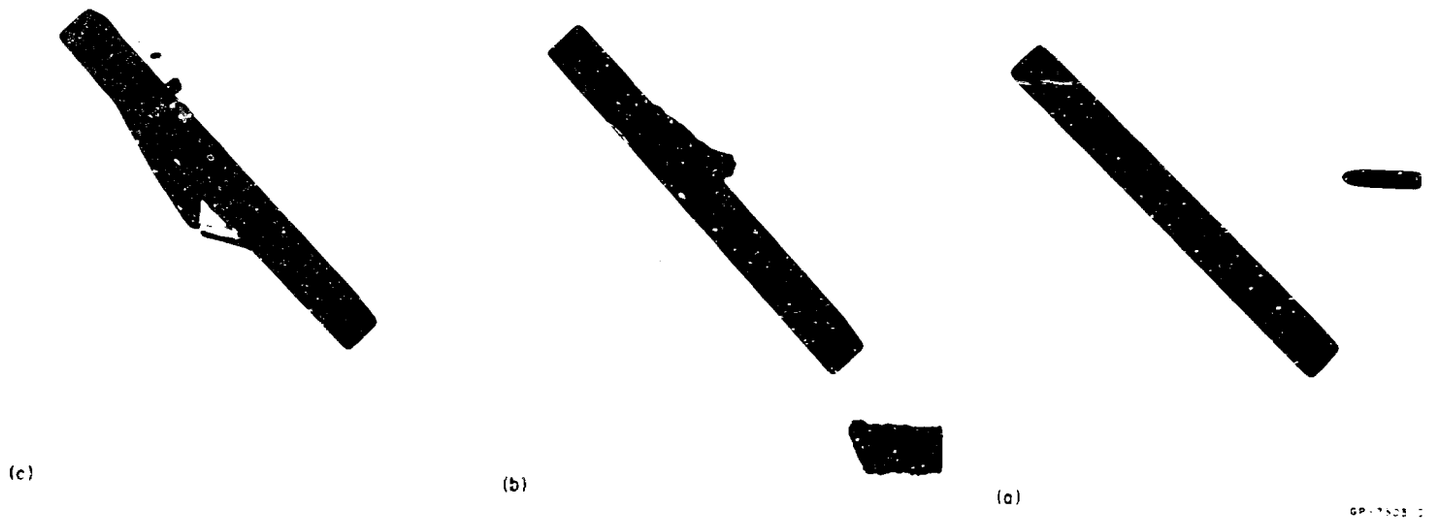

FIGURE 15 IMPACT AT 2400 FT/SEC OF 0.30-CALIBER PROJECTILE AND 0.600-INCH-THICK CERAMIC TILE Angle of Incidence 45°

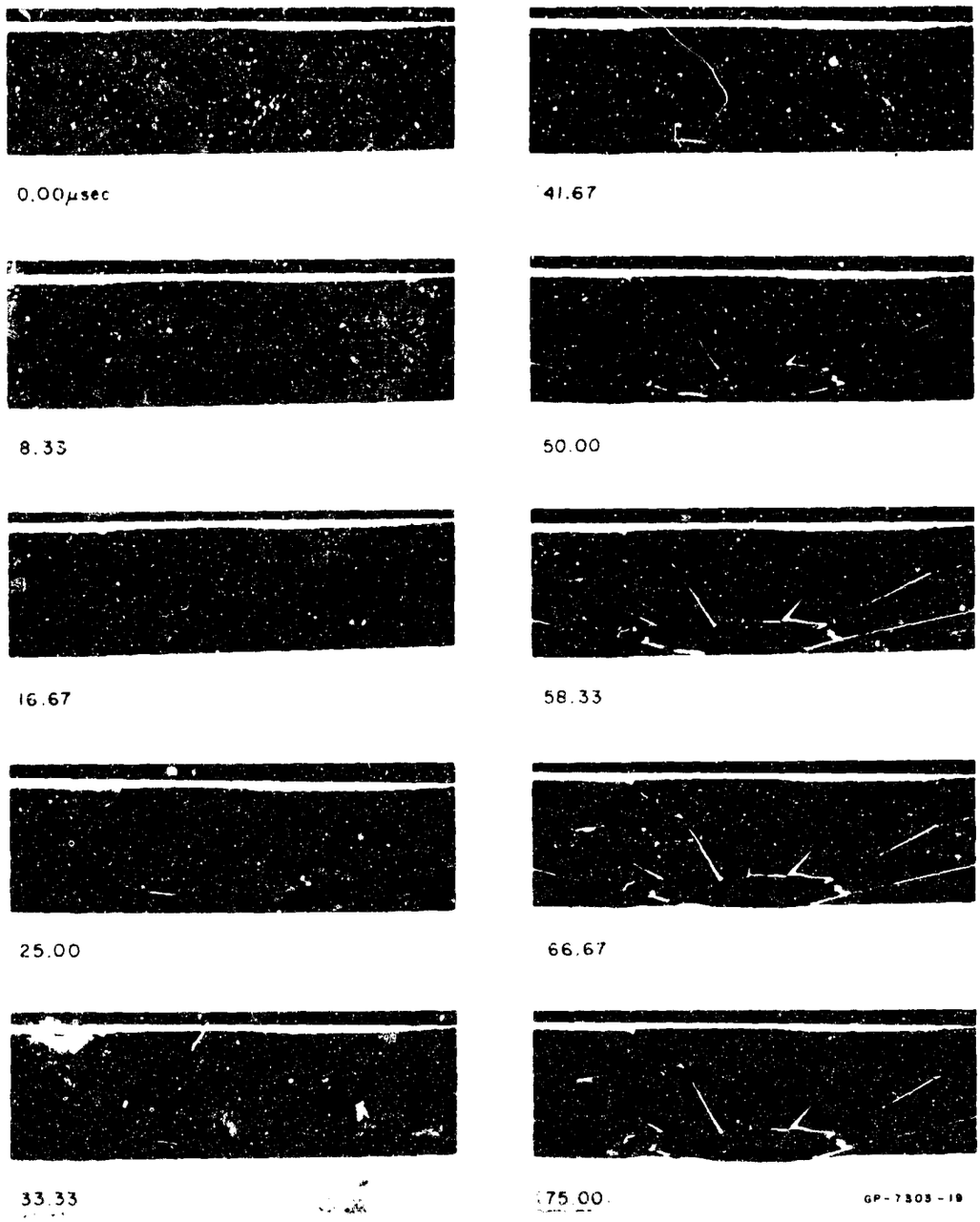

FIGURE 16 OBLIQUE REAR VIEW OF 0.600-INCH-THICK CERAMIC TILE IMPACTED AT 2400 FT/SEC BY 0.30-CALIBER PROJECTILE

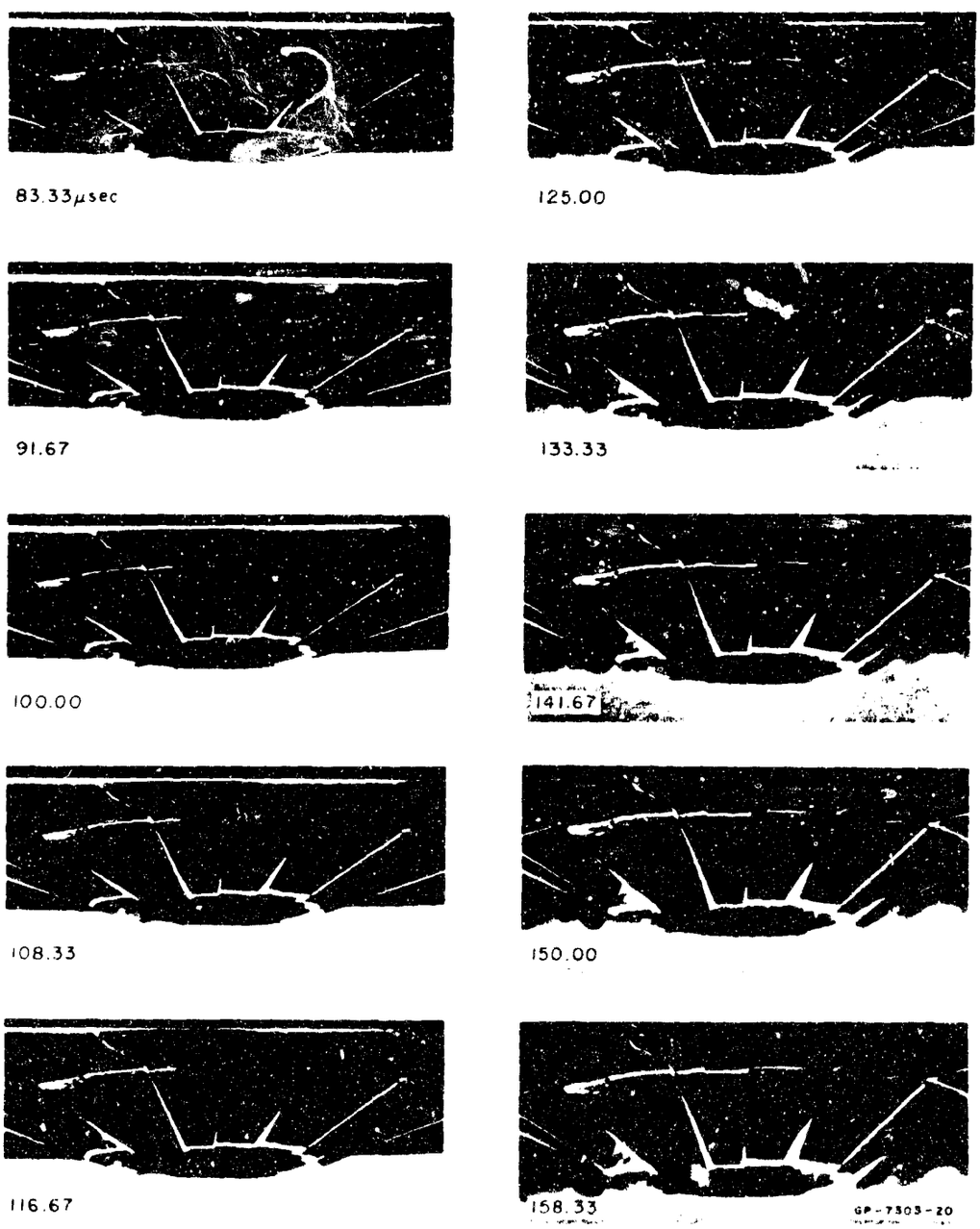

FIGURE 16 OBLIQUE REAR VIEW OF 0.600-INCH-THICK CERAMIC TILE IMPACTED AT 2400 FT/SEC BY 0.30-CALIBER PROJECTILE (Concluded)

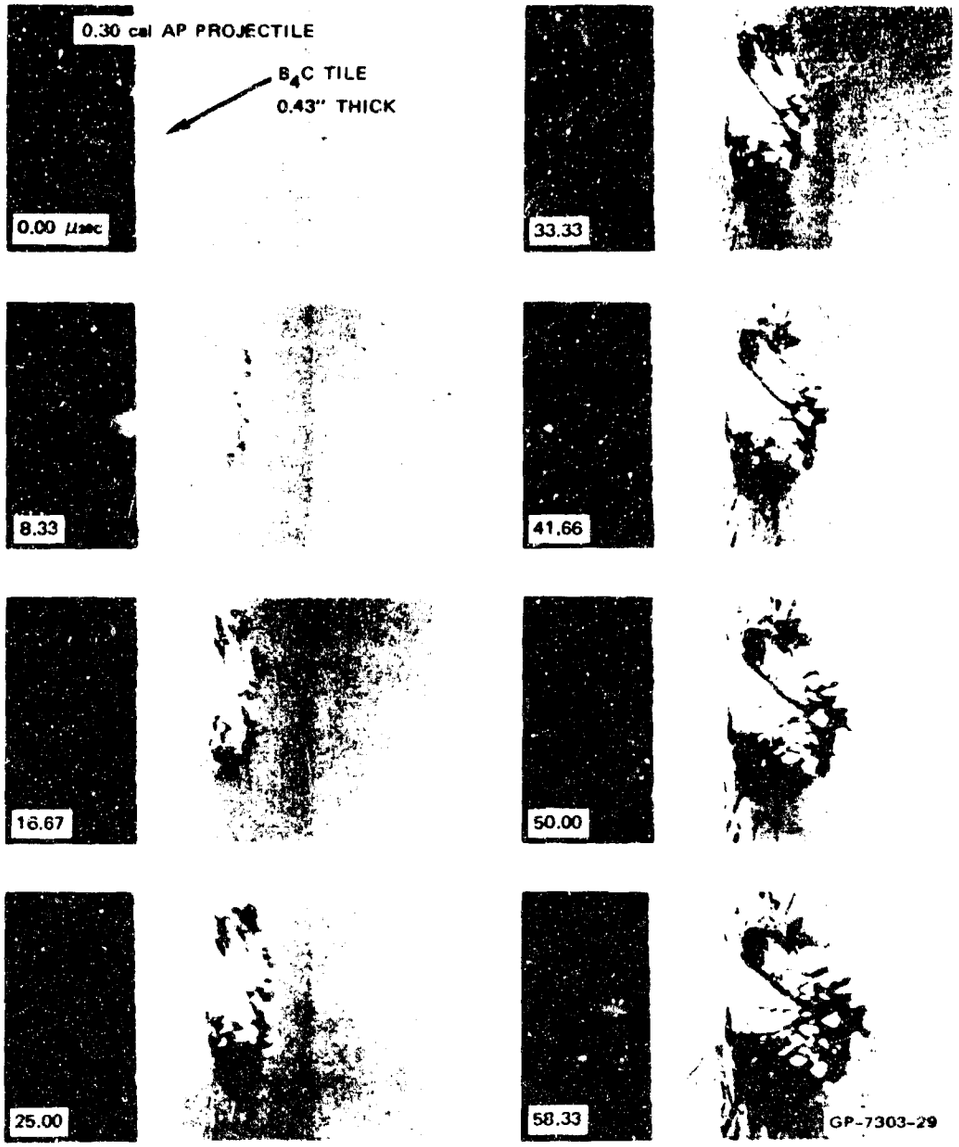

FIGURE 17 OBLIQUE REAR VIEW OF 0.30-CALIBER STANDARD AP PROJECTILE IMPACTING 0.43-INCH-THICK BORON CARBIDE TILE AT 2400 FT/SEC 8.33 μsec Between Frames

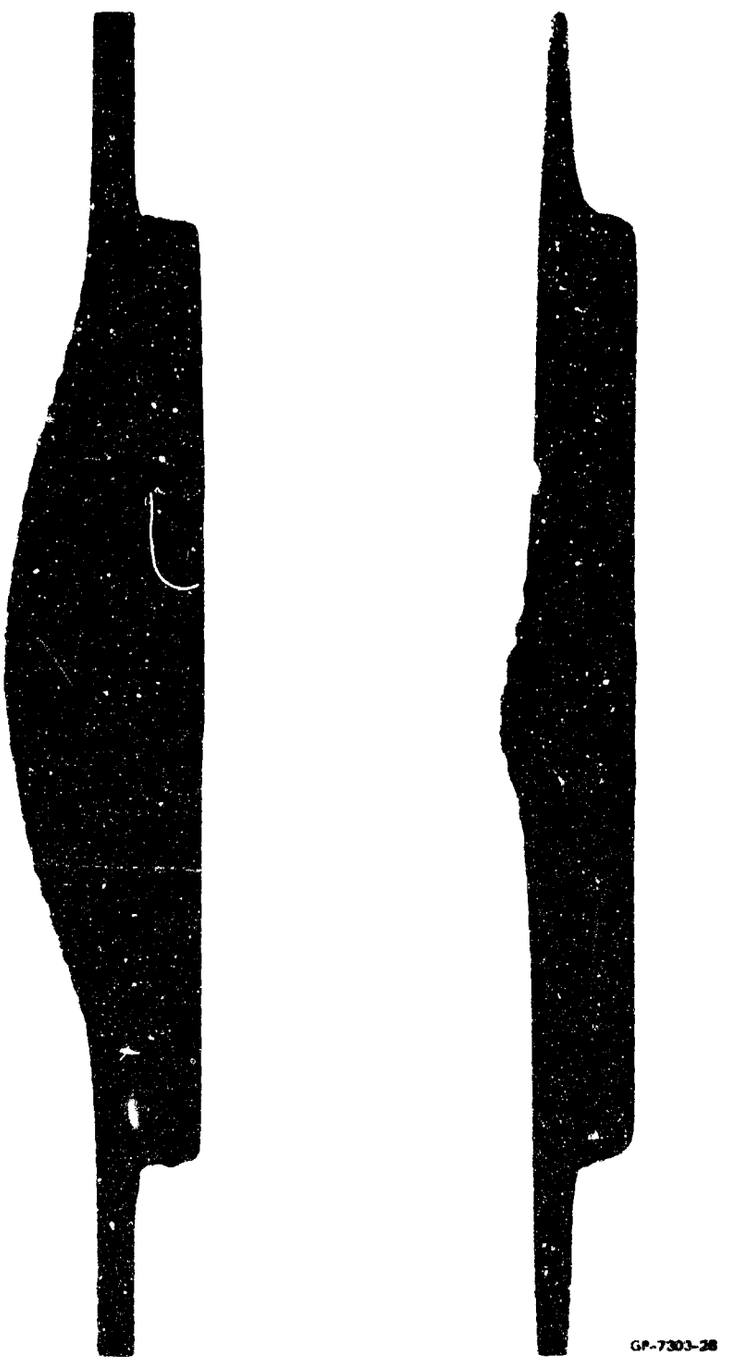

FIGURE 18 IMPACT AT 2400 FT/SEC OF 0.30-CALIBER PROJECTILE AND COMPOSITE ARMOR (0.34-Inch-Thick Aluminum Oxide Bonded to 0.25-Inch-Thick Fiber Glass)

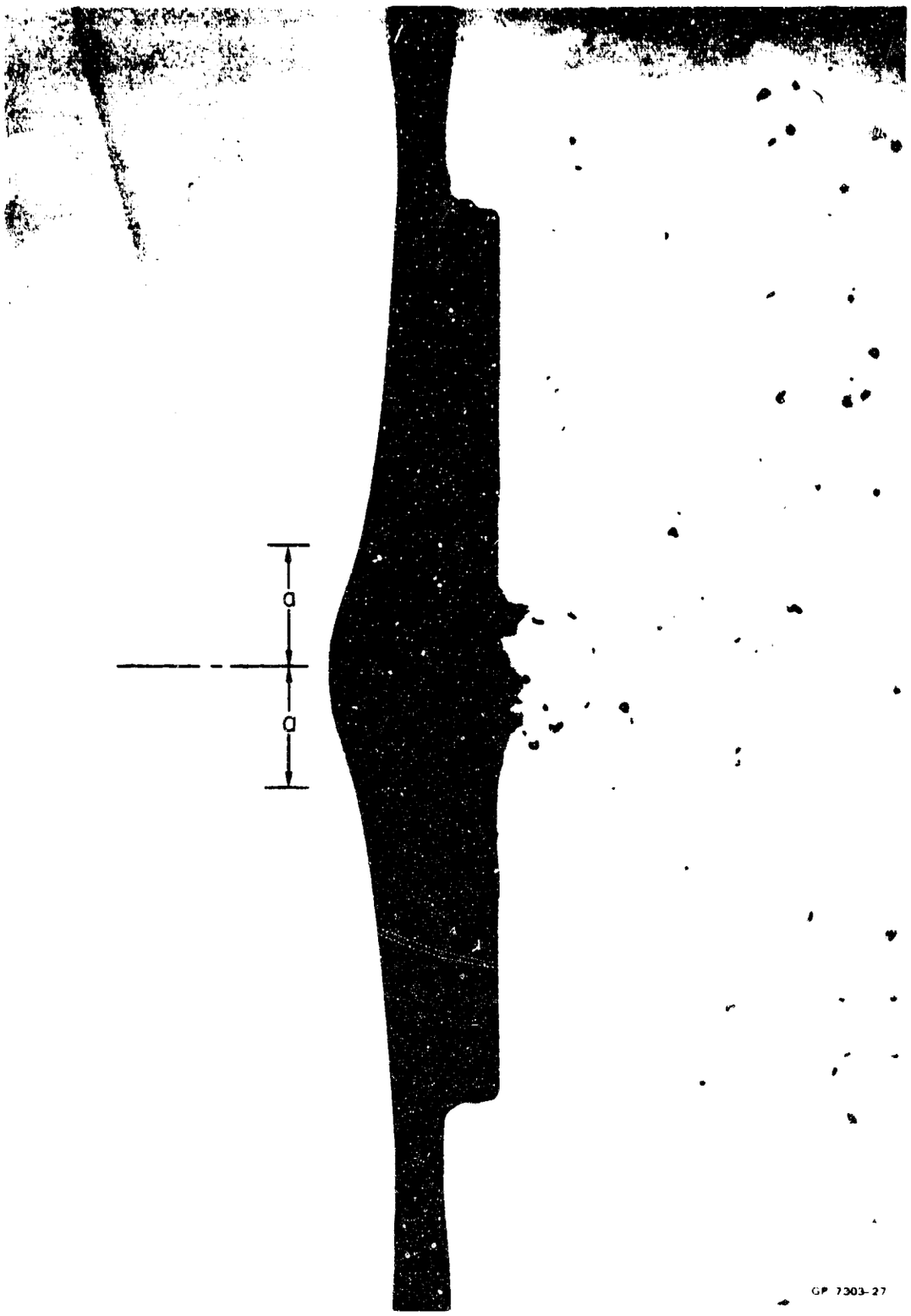

FIGURE 19 IMPACT AT 2400 FT/SEC OF 0.30 CALIBER PROJECTILE AND COMPOSITE ARMOR (0.34 Inch Thick Aluminum Oxide Bonded to 0.25 Inch Thick 6061 T6 Aluminum)

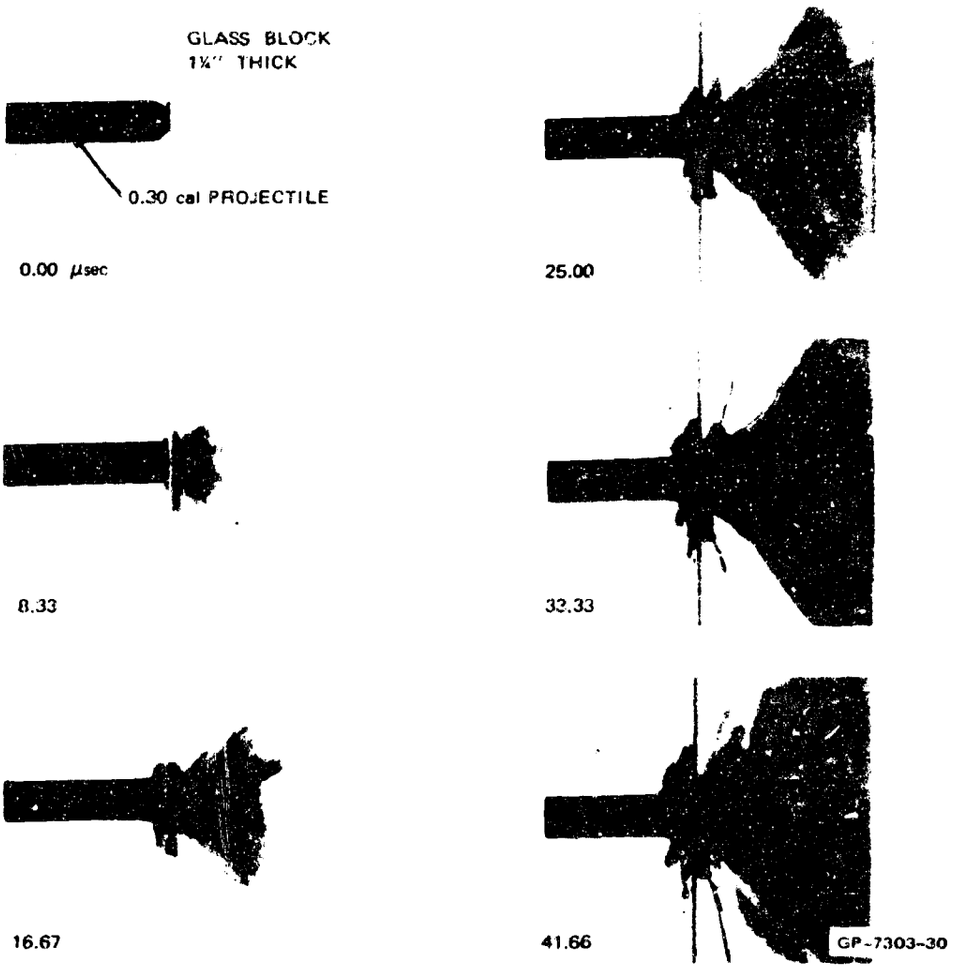

FIGURE 20 CONOIDAL FRACTURE FORMATION IN A 1¼-INCH-THICK GLASS BLOCK IMPACTED AT 350 FT/SEC BY AN 0.30-CALIBER ROUND-NOSE PROJECTILE OF MILD STEEL

V IMPACT STRESSES IN ALUMINUM OXIDE

A. Introduction

An aspect of experimental investigation into projectile-armor interaction that has received little attention is the determination of the stress wave in a facing plate generated by impact. In this section experiments are described and results presented to illustrate the feasibility of measuring the compressive stress profile at the wave front by means of a piezoresistive manganin stress gage. The stress profiles, when correlated with the predictions of computer programs, form a valuable assessment of the constitute equations employed. Another use of the technique is in ascertaining dynamic material properties including fracture behavior. This use requires a one-dimensional or plane strain wave in the facing and is generated by impact with a flat flyer plate.

B. Description of Experiments

A small T-shaped piece of manganin foil 1/2-mil thick is centrally located and sandwiched between two plates of aluminum oxide, as shown in Fig. 21. Electrical leads from the gage pass through holes in the rear plate. The 0.458-inch-diameter hard steel projectile strikes the front plate immediately opposite the gage (Fig. 21a). In the flyer plate experiments a 50-mil-thick steel flyer is driven by sheet explosive* and arranged to strike the entire front surface of the ceramic simultaneously (Fig. 21b). Further details of the experiments, including the circuitry, are contained in Appendix B. Upon reaching the gage the stress wave causes a change in electrical resistance in the manganin, which has a constant current flowing through it, and the resulting increase in voltage across the gage is recorded on oscilloscopes. This

*Detasheet D, manufactured by du Pont.

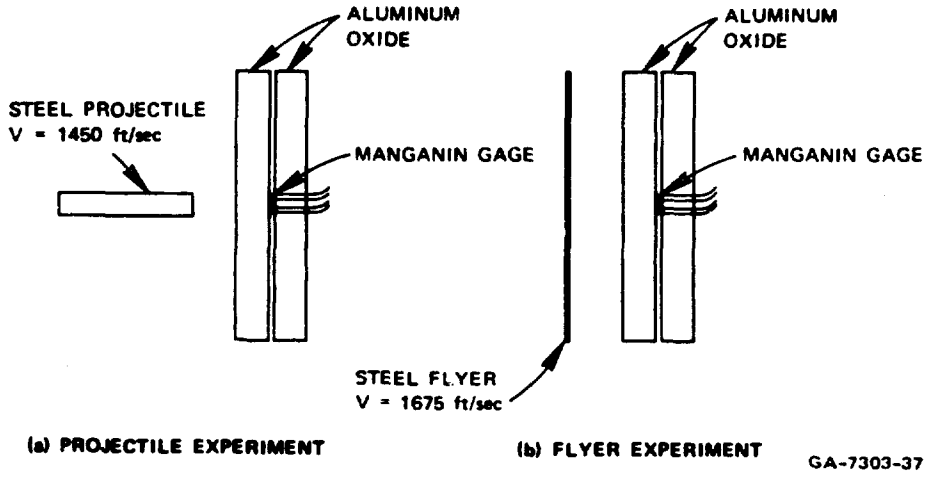

FIGURE 21 SCHEMATIC EXPERIMENTAL ARRANGEMENTS

voltage change is proportional to the stress. The response time of the manganin foil stress gage is about 30 nsec so the wave front is recorded quite accurately.

C. Experimental Results

From the oscillograms, of which two samples are displayed in Fig. 22, the peak stresses listed in Table II were obtained. Peak stresses generated at the impact surface as predicted by one-dimensional linear-elastic theory were 97 and 84 kbar in the flyer and projectile experiments, indicating that peak stresses of about 120 kbar recorded a distance of 0.217 inch from the impact surface are reasonable. Additional confidence in the experimental technique is obtained from the axisymmetric linear-elastic computer program predictions of 90, 70, and 45 kbar at distances of 0.217, 0.375, and 0.540 inch from the projectile (compared with about 123, 72, and 43 kbar in Table II). Also, the decrease in peak stress with distance into the ceramic is much greater in the case of the projectile impact because of the "spherical" divergence of the wave. Another observation is the difference in wave shapes arising in the flyer and projectile experiments as is seen by comparing Figs. 22a and 22b. In the case of flyer impact (Fig. 22a) the stress rises uniformly to a peak stress of 98 kbar in about 0.4 μsec and decays approximately in an exponential manner,

whereas in the case of projectile impact the stress profile exhibits a plateau for about 1.2 μsec before achieving its peak value of 81 kbar. The recording time in both cases is about 4 μsec, which corresponds to the time taken for the wave front to travel to the rear surface of the rear ceramic tile (0.55 inch thick), where it reflects as a tensile wave, and back to the manganin.

D. Conclusions

It is concluded that the above study demonstrates the feasibility of employing manganin stress gages in the study of wave propagation in facing plates of armor caused by projectile impact. The stress gages can also be used for the determination of dynamic material properties by plane wave experiments.

Table II

PEAK STRESSES (kbar) IN ALUMINUM OXIDE

Front Tile Thickness (inch)	Steel Flyer 50-Mils Thick 1675 ft/sec Velocity	Steel Projectile[a] 0.458-Inch Diameter 1450 ft/sec Velocity
0.217	122 121	123
0.375	98 115	63 81
0.550	107	43[b]

[a]Flat-nosed projectile guided for planar impact.

[b]Record quality only fair.

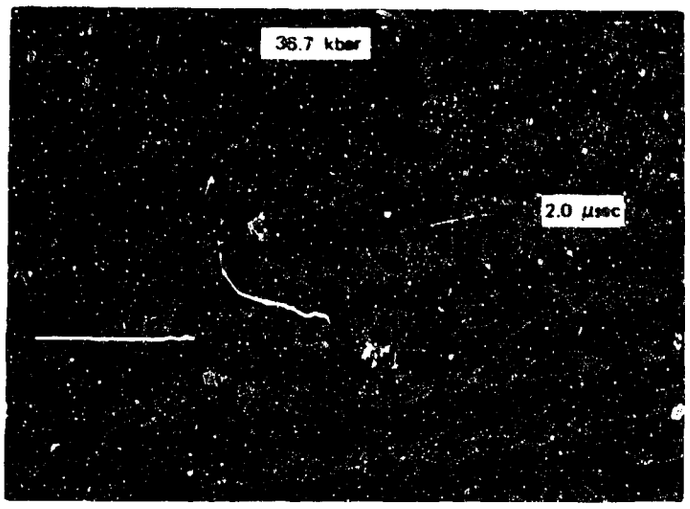

(a) STEEL FLYER, V = 1675 FT/SEC

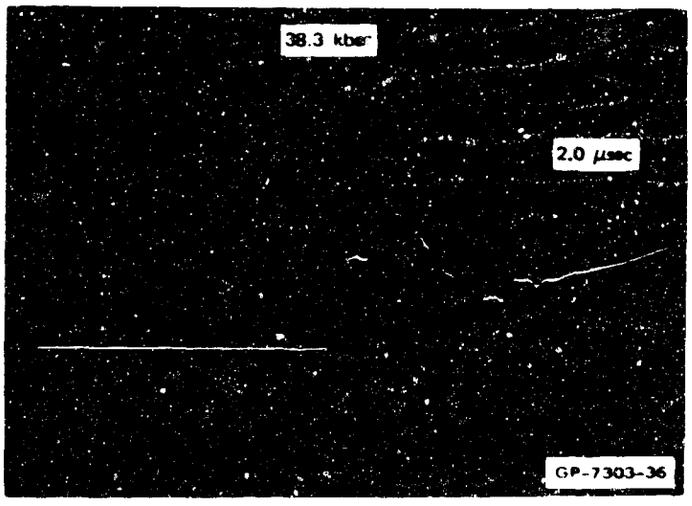

(b) FLAT-NOSED STEEL PROJECTILE, V = 1450 FT/SEC

FIGURE 22 MANGANIN GAGE RECORDS

REFERENCES

1. A. L. Florence and T. J. Ahrens, "Interaction of Projectiles and Composite Armor," Final Report AMRA CR 67-05(F), Contract DA-04-200-AMC-1381(X), Stanford Research Institute, Menlo Park, California, January 31, 1967.

2. M. L. Wilkins, "Third Progress Report of Light Armor Program," Report No. UCRL 50460, Lawrence Radiation Laboratory, University of California, Livermore, California, July 9, 1968.

3. L. D. Bertholf, "Longitudinal Elastic Wave Propagation in Finite Cylindrical Bars," Report No. WSU SDL 66-03, Washington State University, Pullman, Washington, July 1966.

4. L. D. Bertholf, "Numerical Solution for Two-Dimensional Elastic Wave Propagation in Finite Bars," Journal of Applied Mechanics, Vol. 31, No. 3, September 1967, pp. 725-734.

5. L. Seaman and R. K. Linde, "Distended Material Model Development," Vol. I, Final Report, Contract F29601-67-C-0073, Stanford Research Institute, Menlo Park, California, October 26, 1968.

Appendix A

IMPULSIVE MOTION OF AN ELASTIC MEMBRANE

The motion of a uniform membrane of radius a under a constant tension S per unit arc length is governed by the partial differential equation

$$y_{rr} + \frac{1}{r} y_r = \frac{1}{c^2} y_{tt} \qquad \text{(A-1)}$$

where $y(r,t)$ is the transverse deflection and $c^2 = S/m$ (see Fig. A-1a). In (A-1), subscripts denote partial differentiation with respect to the space and time coordinates r and t. The mass m per unit area of membrane is taken to be the sum of the mass m_m per unit area of the membrane itself, a uniform layer of attached mass m_c per unit area (broken up ceramic), and the mass m_p per unit area of a projectile of mass M_p assumed uniformly distributed over the membrane.

The effect of the projectile-ceramic impact is assumed to be the creation of an initial velocity

$$y_t(r,o) = V J_o(\lambda_o r) \qquad \text{(A-2)}$$

as sketched in Fig. A-1b where J_o is a Bessel function of zero order and λ_o is a number such that $J_o(\lambda_o a) = 0$. An initial velocity distribution of this form is not an unreasonable approximation to reality but the particular choice of function is motivated by the simplification that results in the solution of (A-1); (A-2) reduces the solution to the first mode or eigenfunction. The appropriate boundary condition is

$$y(a,t) = 0 \qquad \text{(A-3)}$$

By representing the solution as the product of two functions

$$y(r,t) = R(r)\,T(t) \qquad (A\text{-}4)$$

it follows from (A-1) that

$$R''/R + R'/rR = T''/c^2T = -\lambda^2$$

where the primes denote differentiation and λ is a constant, as yet undetermined. Hence R and T must satisfy the equations

$$R'' + R'/r + \lambda^2 R = 0 \qquad (A\text{-}5)$$

$$T'' + \lambda^2 c^2 T = 0 \qquad (A\text{-}6)$$

The solutions of (A-5) and (A-6) are

$$R = A\,J_o(\lambda r) + B\,Y_o(\lambda r) \qquad (A\text{-}7)$$

$$T = C \sin\lambda ct + D \cos\lambda ct \qquad (A\text{-}8)$$

For a membrane initially at rest, that is, $y(r,o) = 0$, it follows from (A-8) that $D = 0$. Since $Y_o(\lambda r)$ becomes infinite as r approaches zero its coefficient must be set equal to zero for finite displacements at the plate center; hence $B = 0$. The boundary condition (A-3), for nontrivial solutions, is satisfied if $J_o(\lambda a) = 0$, which has infinitely many roots. Naming the n^{th} root λ_n, the solution is

$$y(r,t) = \sum_{o}^{\infty} A_n C_n J_o(\lambda_n r) \sin\lambda_n ct \qquad (A\text{-}9)$$

which represents the sum of the eigenfunctions corresponding to the eigenvalues λ_n.

Time differentiation of (A-9) yields the velocity with the initial value of

$$y_t(r,o) = c \sum_{o}^{\infty} \lambda_n A_n C_n J_o(\lambda_n r) \qquad (A-10)$$

Since the specified initial velocity is (A-2), it follows from the orthogonality property of the eigenfunctions $J_o(\lambda_n r)$ that $c\lambda_o A_o B_o = V$ and $A_n B_n = 0, \quad n \neq 0$. Hence

$$y(r,t) = [Va/c(\lambda_o a)]J_o(\lambda_o r) \sin\lambda_o ct \qquad (A-11)$$

where the first zero of $J_o(\lambda_o a)$ gives $\lambda_o a = 2.405$.

The maximum deflection δ occurs at the center when motion ceases at time $t = \pi a/c(\lambda_o a)$ and since $J_o(o) = 1$, (A-11) gives

$$\delta = Va/c(\lambda_o a)$$

Space differentiation of (A-11) yields the slope y_r which has a magnitude maximum ϑ at a radius r_m given by $\max[-J_o'(\lambda_o r)] = \max J_1(\lambda_o r) = 0.582$ and at time $t = \pi a/c(\lambda_o a)$. Thus $r_m/a = \lambda_o r_m/\lambda_o a \approx 1.8/2.4 = 0.75$ and

$$\vartheta = (V/c) \cdot J_1(\lambda_o r_m) \qquad (A-12)$$

The radial strain ε_r in the membrane can be shown to be $y_r^2/2$. Consequently, by (A-12), the maximum strain is

$$\max \varepsilon_r = (V/c)^2 J_1^2(\lambda_o r_m)\, 2 \qquad (A-13)$$

The velocity V is now related to the projectile velocity V_p and mass M_p by equating the initial momentum of the membrane to the projectile momentum. Thus

$$\int_o^a mV J_o(\lambda_o r) \cdot 2\pi r \, dr = M_p V_p$$

which gives

$$V = [m_p/(m_m + m_c + m_p)][(\lambda_o a)/2J_1(\lambda_o a)]V_p \qquad (A\text{-}14)$$

By substituting V from (A-14) and $c^2 = S/m = S/(m_m + m_c + m_p)$ into (A-13) the maximum strain expression becomes

$$\max \varepsilon_r = [(\lambda_o a)J_1(\lambda_o r_m)/2J_1(\lambda_o a)]^2[m_p^2/(m_m + m_c + m_p)]V_p^2/2S \qquad (A\text{-}15)$$

Finally, to exhibit the effect of the membrane radius upon the maximum strain, (A-15) is written as

$$\max \varepsilon_r = [(\lambda_o a)J_1(\lambda_o r_m)/2J_1(\lambda_o a)]^2[M_p/\{M_p + (m_m + m_c)\pi a^2\}](M_p V^2/2)/2S \qquad (A\text{-}16)$$

The above analysis is applicable to a rigid-perfectly plastic membrane of maximum permissible tension S because the choice of initial velocity distribution ensures loading of all membrane elements until the motion ceases. Thereafter, unloading occurs and the theory is no longer applicable to a rigid-plastic membrane. However, our interest is in the first loading phase of the membrane.

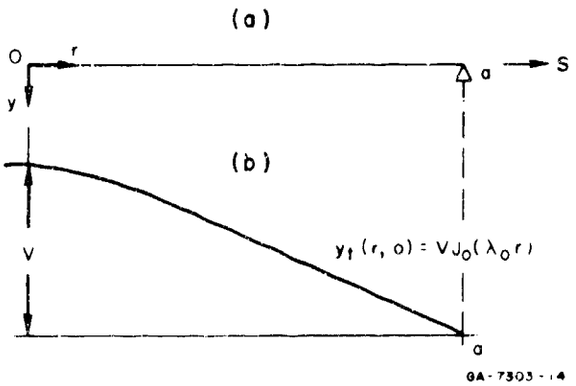

FIGURE A-1 STRETCHED CIRCULAR MEMBRANE
(a) Coordinates, (b) Initial Velocity Distribution

Appendix B

PRESSURE MEASUREMENTS WITH MANGANIN GAGES

A. Introduction

The experimental method used to measure dynamic pressure makes use of the piezoresistive property of manganin. For the pressure range of interest in projectile-armor impact the pressure-resistance relationship in manganin is linear and well-defined. This relationship is

$$p = \frac{1}{k}\frac{\Delta R}{R}$$

where p is pressure in kbar, $k = 0.0028\ \text{kbar}^{-1}$, ΔR is the change in electrical resistance due to the change in pressure, and R is the initial resistance of the specimen. In this stress range electrical inductance effects are small. Hence, for a manganin specimen through which a slowly varying current is flowing, the fractional change in resistance due to a change in pressure is well-approximated by the fractional change in voltage across the specimen. The dynamic pressure is thus determined by measuring the fractional change in voltage and employing the relation

$$p = \frac{1}{k}\frac{\Delta V}{V} \qquad \text{(B-1)}$$

where ΔV is the change in voltage due to the change in pressure and V is the initial voltage.

Manganin is embedded in the material through which the pressure pulse travels. Since the manganin pressure-resistance relationship is independent of temperature and insensitive to final pressure and volume, Eq. (B-1) is valid for any embedding material. Measurements reported in Section V were made with manganin foil sandwiched between two ceramic tiles.

B. Fabrication

Figure B-1a shows the layered construction of the manganin-ceramic gage. The manganin, a one-piece ⁻ pattern (Fig. B-1b) of 0.0005-inch-thick foil, is sandwiched between two 3-inch square ceramic tiles. The gage is constructed by drilling four holes in one tile at points corresponding to the four tips of the ⁻ pattern. The manganin foil is then bonded to the tile with a thin layer of C-7 epoxy and the tips of the foil are bent down into the holes; the holes are then filled with an electrically conducting dental amalgum. Copper wires are embedded in the amalgum from the back side of the tile providing four electrical connections to the manganin foil. The second tile is then bonded to the first tile with another thin layer of C-7 epoxy to complete the gage construction.

C. Experimental Arrangements

For gages impacted by steel flyer plates the experimental configuration shown in Fig. B-2 was used. The flyer plate covered with sheet explosive is suspended above the gage by four thin aluminum tabs attached to a wooden frame (Fig. B-2a). Detonation of the explosive accelerates the flyer plate toward the gage but also causes the plate to undergo an angular displacement. To achieve a simultaneous impact the gage is tilted by this same angle during the experimental setup as shown in Fig. 2b.

For gages impacted by a flat-nosed steel projectile, the experimental configuration shown in Fig. B-3 was used. After the projectile leaves the barrel its flight is confined by three parallel steel guides spaced 120° apart circumferentially around the projectile. This assures a planar impact between the nose of the projectile and the target face. Before the projectile impinges on the target it passes through an electrical switch that triggers the measuring circuit.

D. Instrumentation

The resistance of the manganin foil as a functio of time is determined by measuring the voltage across the manganin specimen

through which a constant current is flowing. This is accomplished with the circuit illustrated schematically in Fig. B-4.

The power supply is an RC circuit with a time constant much longer than the duration of the pressure pulses of interest. A D.C. power supply charges the capacitor. Closing switch 1 discharges the capacitor through a 26-kΩ resistor and through the power leads to the manganin foil providing a nearly constant current through the foil. For flying plate experiments switch 1 is closed at the same time an electrical pulse is applied to the detonator. For flat-nosed projectile experiments switch 1 is closed when the projectile strikes the triggering switch. The power supply remains on for a preset duration and is then shorted out by closing switch 2 after the pressure pulse has passed the sensing element of the gage. Hence a nearly constant current is flowing through the foil for the duration of the pressure pulse.

The voltage across the sensing element of the manganin foil is measured across the signal leads. Oscilloscope 1 displays the voltage across the signal leads beginning just before the power supply is turned on and ending just after it is turned off. The arrival of the pressure pulse is illustrated on oscilloscope 1 in Fig. B-4.

A more accurate measurement of the amplitude of the pressure pulse is made by oscilloscope 2. This displays the difference between the signal shown on oscilloscope 1 and the same signal that has been delayed; displacement on oscilloscope 2 is due only to the pressure pulse itself and not to the turn-on voltage. By employing this technique the offset voltage can be amplified for more accurate measurement.

Permanent records of the oscilloscope displays are obtained by Polaroid cameras attached to the oscilloscopes. The initial voltage V is read from oscilloscope 1 and the change in voltage ΔV is read from oscilloscope 2. The pressure is calculated from Eq. (B-1).

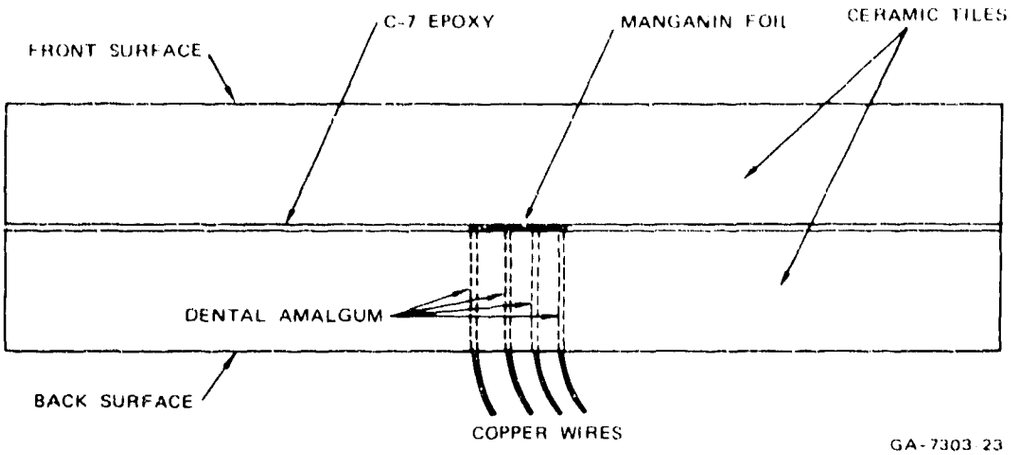

(a) ASSEMBLY CONFIGURATION

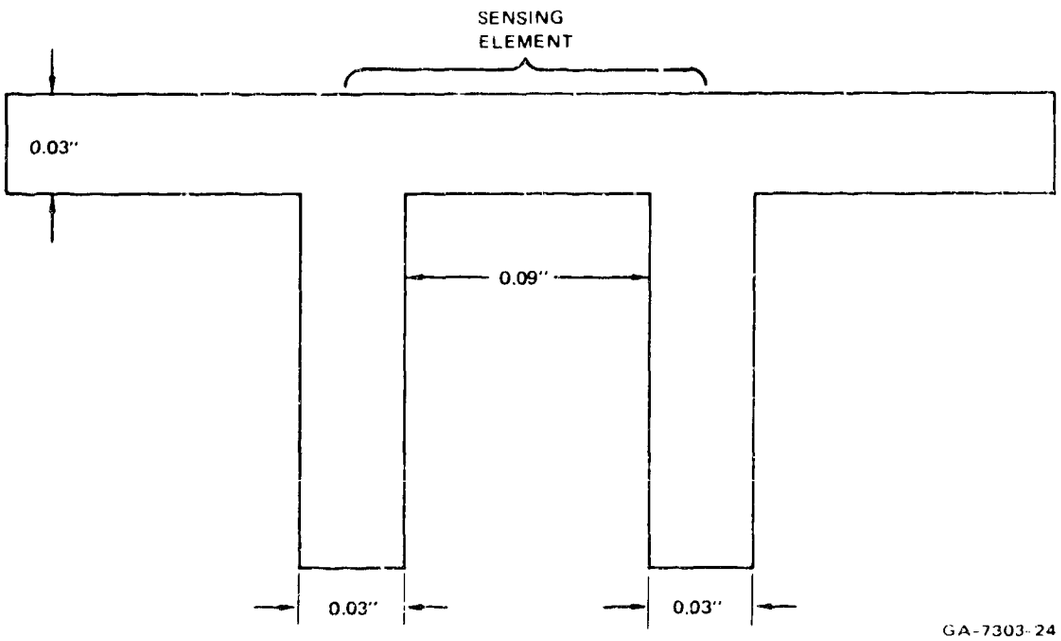

(b) MANGANIN FOIL π PATTERN

FIGURE B-1 MANGANIN-CERAMIC GAGE

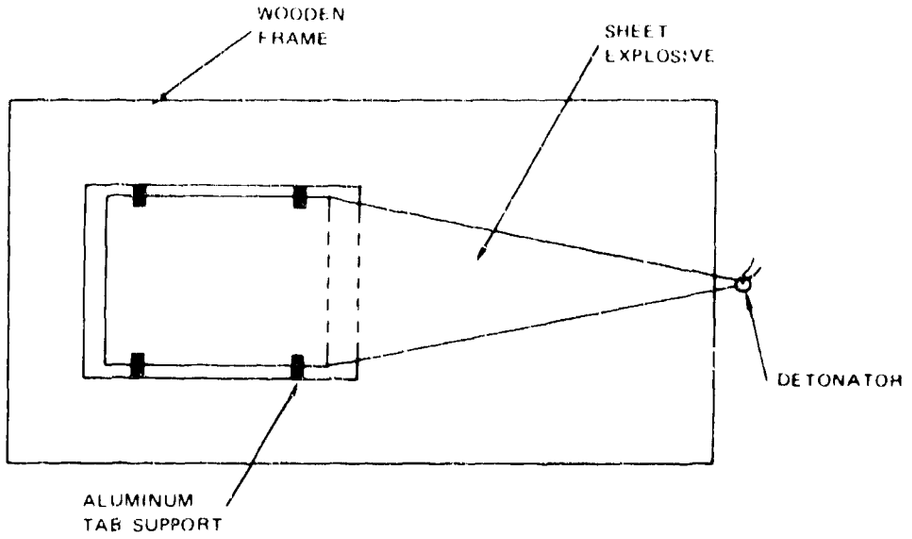

(a)

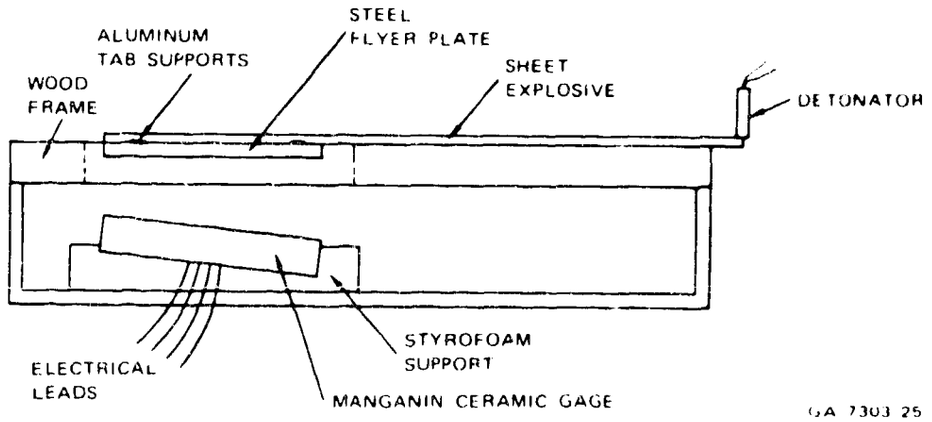

(b)

FIGURE B-2 EXPERIMENTAL CONFIGURATION FOR FLYING PLATES

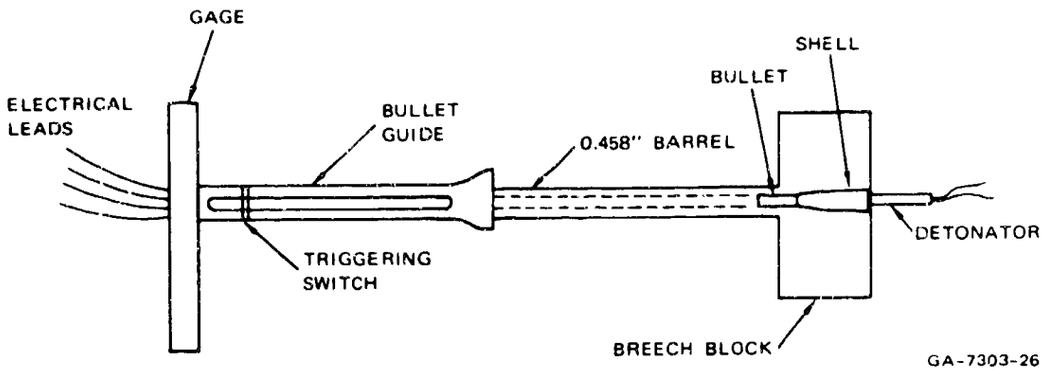

FIGURE B-3 EXPERIMENTAL CONFIGURATION FOR FLAT-NOSED PROJECTILES

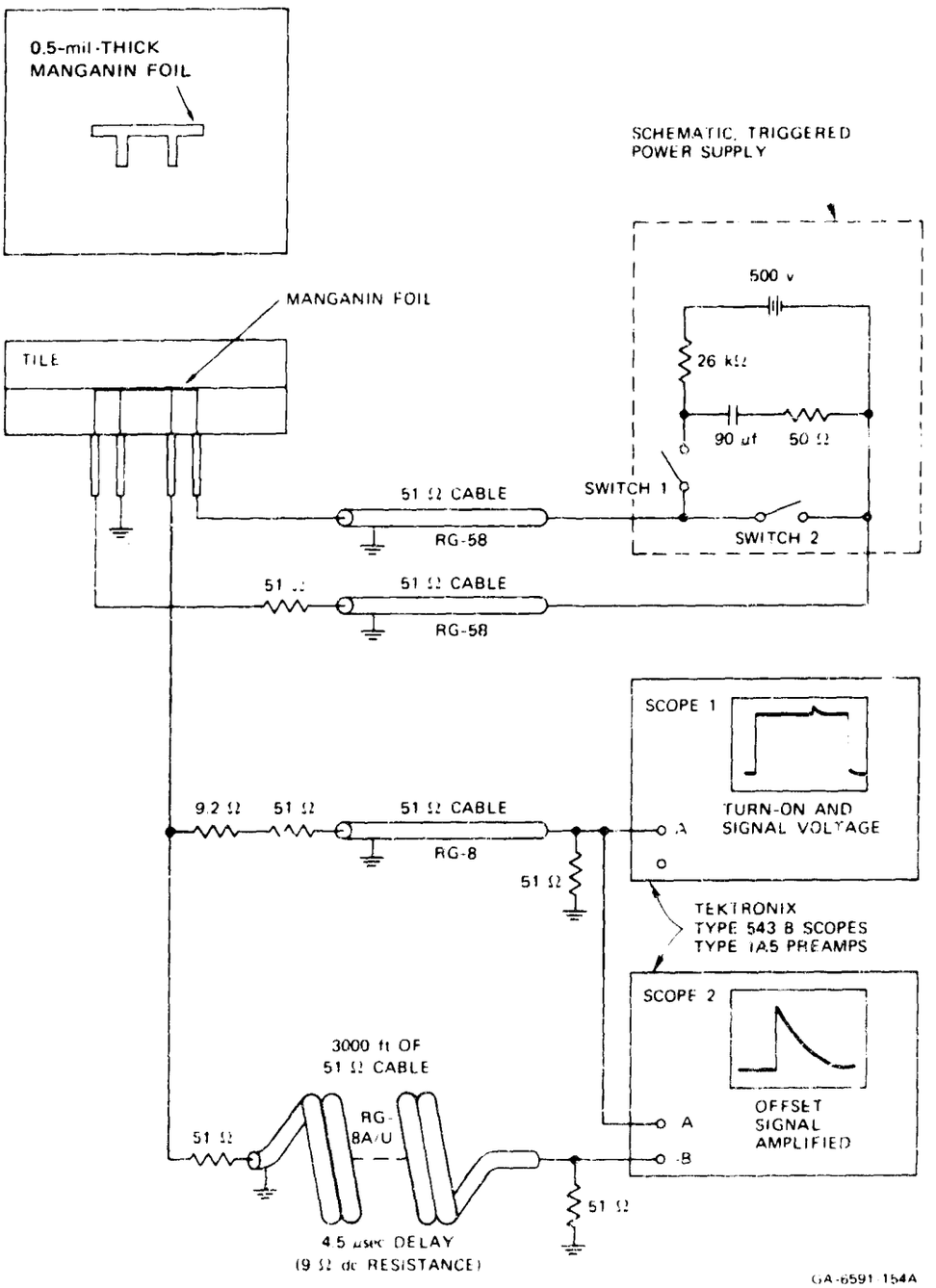

FIGURE B-4 ELECTRICAL CIRCUITRY FOR DISPLAYING VOLTAGE AND VOLTAGE CHANGE (V and ΔV)

UNCLASSIFIED

Security Classification

DOCUMENT CONTROL DATA - R & D

Security classification of title, body of abstract and indexing annotation must be entered when the overall report is classified

1 ORIGINATING ACTIVITY (Corporate author)	2a. REPORT SECURITY CLASSIFICATION
Stanford Research Institute 333 Ravenswood Avenue Menlo Park, California 94025	Unclassified 2b. GROUP

3 REPORT TITLE

INTERACTION OF PROJECTILES AND COMPOSITE ARMOR, PART II

4 DESCRIPTIVE NOTES (*Type of report and inclusive dates*)

Final Report - April 25, 1968 - April 25, 1969

5 AUTHOR(S) (*First name, middle initial, last name*)

Alexander L. Florence

6 REPORT DATE	7a. TOTAL NO OF PAGES	7b. NO OF REFS
August 1969	76	5

8a CONTRACT OR GRANT NO	9a. ORIGINATOR'S REPORT NUMBER(S)
DAAG46-68-C-0054 b. PROJECT NO c. d.	AMMRC CR 69-15 9b. OTHER REPORT NO(S) (*Any other numbers that may be assigned this report*) SRI Project PGU 7303

10 DISTRIBUTION STATEMENT

This document has been approved for public release and sale; its distribution is unlimited.

11 SUPPLEMENTARY NOTES	12 SPONSORING MILITARY ACTIVITY
	Army Materials and Mechanics Research Center Watertown, Massachusetts 02172

13 ABSTRACT

This report describes basic experimental and theoretical investigations of the interaction of projectiles and lightweight armor. The armor of interest is a very hard and relatively inflexible facing plate (ceramic) bonded to a flexible backing plate (fiber glass or aluminum alloy).

The theoretical work concerns: (1) development of an analytical model for describing the restraining mechanisms of the armor and for prediction of ballistic limits, (2) checkout and use of a simple computer code for obtaining stress fields in brittle facing plates and projectiles caused by impact at normal incidence.

The experimental work concerns: (1) the use of high-speed photography and flash X-ray techniques for specific investigations such as observing fracture conoids in facing plates, (2) demonstrating that stresses in ceramic facing plates can be measured by manganin stress gages.

DD FORM 1 NOV 1473 (PAGE 1)

S/N 0101-807-6801

UNCLASSIFIED

Security Classification

AD ________ Accession No. ________
Army Materials and Mechanics Research Center, Watertown, Massachusetts 02172

INTERACTION OF PROJECTILES AND COMPOSITE ARMOR, Part II, A. L. Florence, Stanford Research Institute, Menlo Park, California 94025

Technical Report AMMRC CR 69-15, August 1969, 76 pp. illus - tables, Contract DAAG46-68-C-0054, Final Report, Apr 68 - Apr 69, Unclassified Report

This report describes basic experimental and theoretical investigations of the interaction of projectiles and light-weight armor. The armor of interest is a very hard and relatively inflexible facing plate (ceramic) bonded to a flexible backing plate (fiber glass or aluminum alloy).

The theoretical work concerns: (1) development of an analytical model for describing the restraining mechanisms of the armor and for prediction of ballistic limits; (2) checkout and use of a simple computer code for obtaining stress fields in brittle facing plates and

UNCLASSIFIED

1. Armor
2. Lightweight Armor
3. Ceramic Armor
4. Fiberglass
5. Fracture Conoid
6. Manganin Stress Gage
7. Stress Waves
8. Steel Projectiles
9. Composite Armor
I Florence, A. L.
II Stanford Research Institute

AD ________ Accession No. ________
Army Materials and Mechanics Research Center, Watertown, Massachusetts 02172

INTERACTION OF PROJECTILES AND COMPOSITE ARMOR, Part II, A. L. Florence, Stanford Research Institute, Menlo Park, California 94025

Technical Report AMMRC CR 69-15, August 1969, 76 pp. illus - tables, Contract DAAG46-68-C-0054, Final Report, Apr 68 - Apr 69, Unclassified Report

This report describes basic experimental and theoretical investigations of the interaction of projectiles and light-weight armor. The armor of interest is a very hard and relatively inflexible facing plate (ceramic) bonded to a flexible backing plate (fiber glass or aluminum alloy).

The theoretical work concerns: (1) development of an analytical model for describing the restraining mechanisms of the armor and for prediction of ballistic limits; (2) checkout and use of a simple computer code for obtaining stress fields in brittle facing plates and

UNCLASSIFIED

1. Armor
2. Lightweight Armor
3. Ceramic Armor
4. Fiberglass
5. Fracture Conoid
6. Manganin Stress Gage
7. Stress Waves
8. Steel Projectiles
9. Composite Armor
I Florence, A. L.
II Stanford Research Institute

AD ________ Accession No. ________
Army Materials and Mechanics Research Center, Watertown, Massachusetts 02172

INTERACTION OF PROJECTILES AND COMPOSITE ARMOR, Part II, A. L. Florence, Stanford Research Institute, Menlo Park, California 94025

Technical Report AMMRC CR 69-15, August 1969, 76 pp. illus - tables, Contract DAAG46-68-C-0054, Final Report, Apr 68 - Apr 69, Unclassified Report

This report describes basic experimental and theoretical investigations of the interaction of projectiles and light-weight armor. The armor of interest is a very hard and relatively inflexible facing plate (ceramic) bonded to a flexible backing plate (fiber glass or aluminum alloy).

The theoretical work concerns: (1) development of an analytical model for describing the restraining mechanisms of the armor and for prediction of ballistic limits; (2) checkout and use of a simple computer code for obtaining stress fields in brittle facing plates and

UNCLASSIFIED

1. Armor
2. Lightweight Armor
3. Ceramic Armor
4. Fiberglass
5. Fracture Conoid
6. Manganin Stress Gage
7. Stress Waves
8. Steel Projectiles
9. Composite Armor
I Florence, A. L.
II Stanford Research Institute

AD ________ Accession No. ________
Army Materials and Mechanics Research Center, Watertown, Massachusetts 02172

INTERACTION OF PROJECTILES AND COMPOSITE ARMOR, Part II, A. L. Florence, Stanford Research Institute, Menlo Park, California 94025

Technical Report AMMRC CR 69-15, August 1969, 76 pp. illus - tables, Contract DAAG46-68-C-0054, Final Report, Apr 68 - Apr 69, Unclassified Report

This report describes basic experimental and theoretical investigations of the interaction of projectiles and light-weight armor. The armor of interest is a very hard and relatively inflexible facing plate (ceramic) bonded to a flexible backing plate (fiber glass or aluminum alloy).

The theoretical work concerns: (1) development of an analytical model for describing the restraining mechanisms of the armor and for prediction of ballistic limits; (2) checkout and use of a simple computer code for obtaining stress fields in brittle facing plates and

UNCLASSIFIED

1. Armor
2. Lightweight Armor
3. Ceramic Armor
4. Fiberglass
5. Fracture Conoid
6. Manganin Stress Gage
7. Stress Waves
8. Steel Projectiles
9. Composite Armor
I Florence, A. L.
II Stanford Research Institute

AD ______________ Accession No. ______________
Army Materials and Mechanics Research Center, Watertown, Massachusetts 02172

INTERACTION OF PROJECTILES AND COMPOSITE ARMOR, Part II, A. L. Florence, Stanford Research Institute, Menlo Park, California 94025

Technical Report AMMRC CR 69-15, August 1969, 76 pp. illus - tables, Contract DAAG46-68-C-0054, Final Report, Apr 68 - Apr 69, Unclassified Report

This report describes basic experimental and theoretical investigations of the interaction of projectiles and light-weight armor. The armor of interest is a very hard and relatively inflexible facing plate (ceramic) bonded to a flexible backing plate (fiber glass or aluminum alloy).

The theoretical work concerns: (1) development of an analytical model for describing the restraining mechanisms of the armor and for prediction of ballistic limits; (2) checkout and use of a simple computer code for obtaining stress fields in brittle facing plates and

UNCLASSIFIED

1. Armor
2. Lightweight Armor
3. Ceramic Armor
4. Fiberglass
5. Fracture Conoid
6. Manganin Stress Gage
7. Stress Waves
8. Steel Projectiles
9. Composite Armor
I Florence, A. L.
II Stanford Research Institute

AD ______________ Accession No. ______________
Army Materials and Mechanics Research Center, Watertown, Massachusetts 02172

INTERACTION OF PROJECTILES AND COMPOSITE ARMOR, Part II, A. L. Florence, Stanford Research Institute, Menlo Park, California 94025

Technical Report AMMRC CR 69-15, August 1969, 76 pp. illus - tables, Contract DAAG46-68-C-0054, Final Report, Apr 68 - Apr 69, Unclassified Report

This report describes basic experimental and theoretical investigations of the interaction of projectiles and light-weight armor. The armor of interest is a very hard and relatively inflexible facing plate (ceramic) bonded to a flexible backing plate (fiber glass or aluminum alloy).

The theoretical work concerns: (1) development of an analytical model for describing the restraining mechanisms of the armor and for prediction of ballistic limits; (2) checkout and use of a simple computer code for obtaining stress fields in brittle facing plates and

UNCLASSIFIED

1. Armor
2. Lightweight Armor
3. Ceramic Armor
4. Fiberglass
5. Fracture Conoid
6. Manganin Stress Gage
7. Stress Waves
8. Steel Projectiles
9. Composite Armor
I Florence, A. L.
II Stanford Research Institute

AD ______________ Accession No. ______________
Army Materials and Mechanics Research Center, Watertown, Massachusetts 02172

INTERACTION OF PROJECTILES AND COMPOSITE ARMOR, Part II, A. L. Florence, Stanford Research Institute, Menlo Park, California 94025

Technical Report AMMRC CR 69-15, August 1969, 76 pp. illus - tables, Contract DAAG46-68-C-0054, Final Report, Apr 68 - Apr 69, Unclassified Report

This report describes basic experimental and theoretical investigations of the interaction of projectiles and light-weight armor. The armor of interest is a very hard and relatively inflexible facing plate (ceramic) bonded to a flexible backing plate (fiber glass or aluminum alloy).

The theoretical work concerns: (1) development of an analytical model for describing the restraining mechanisms of the armor and for prediction of ballistic limits; (2) checkout and use of a simple computer code for obtaining stress fields in brittle facing plates and

UNCLASSIFIED

1. Armor
2. Lightweight Armor
3. Ceramic Armor
4. Fiberglass
5. Fracture Conoid
6. Manganin Stress Gage
7. Stress Waves
8. Steel Projectiles
9. Composite Armor
I Florence, A. L.
II Stanford Research Institute

AD ______________ Accession No. ______________
Army Materials and Mechanics Research Center, Watertown, Massachusetts 02172

INTERACTION OF PROJECTILES AND COMPOSITE ARMOR, Part II, A. L. Florence, Stanford Research Institute, Menlo Park, California 94025

Technical Report AMMRC CR 69-15, August 1969, 76 pp. illus - tables, Contract DAAG46-68-C-0054, Final Report, Apr 68 - Apr 69, Unclassified Report

This report describes basic experimental and theoretical investigations of the interaction of projectiles and light-weight armor. The armor of interest is a very hard and relatively inflexible facing plate (ceramic) bonded to a flexible backing plate (fiber glass or aluminum alloy).

The theoretical work concerns: (1) development of an analytical model for describing the restraining mechanisms of the armor and for prediction of ballistic limits; (2) checkout and use of a simple computer code for obtaining stress fields in brittle facing plates and

UNCLASSIFIED

1. Armor
2. Lightweight Armor
3. Ceramic Armor
4. Fiberglass
5. Fracture Conoid
6. Manganin Stress Gage
7. Stress Waves
8. Steel Projectiles
9. Composite Armor
I Florence, A. L.
II Stanford Research Institute

projectiles caused by impact at normal incidence. The experimental work concerns: (1) the use of high-speed photography and flash X-ray techniques for specific investigations such as observing fracture conoids in facing plates; (2) demonstrating that stresses in ceramic facing plates can be measured by manganin stress gages.	III Contract DAAG46-68-C-0054 UNCLASSIFIED	projectiles caused by impact at normal incidence. The experimental work concerns: (1) the use of high-speed photography and flash X-ray techniques for specific investigations such as observing fracture conoids in facing plates; (2) demonstrating that stresses in ceramic facing plates can be measured by manganin stress gages.	III Contract DAAG46-68-C-0054 UNCLASSIFIED
projectiles caused by impact at normal incidence. The experimental work concerns: (1) the use of high-speed photography and flash X-ray techniques for specific investigations such as observing fracture conoids in facing plates; (2) demonstrating that stresses in ceramic facing plates can be measured by manganin stress gages.	III Contract DAAG46-68-C-0054 UNCLASSIFIED	projectiles caused by impact at normal incidence. The experimental work concerns: (1) the use of high-speed photography and flash X-ray techniques for specific investigations such as observing fracture conoids in facing plates; (2) demonstrating that stresses in ceramic facing plates can be measured by manganin stress gages.	III Contract DAAG46-68-C-0054 UNCLASSIFIED

UNCLASSIFIED

Security Classification

14 KEY WORDS	LINK A		LINK B		LINK C	
	ROLE	WT	ROLE	WT	ROLE	WT
Armor						
Lightweight armor						
Ceramic armor						
Fiberglass						
Fracture conoid						
Manganin stress gage						
Stress waves						
Steel projectiles						
Composite armor						

DD FORM 1 NOV 65 1473 (BACK)

(PAGE 2)

UNCLASSIFIED

Security Classification